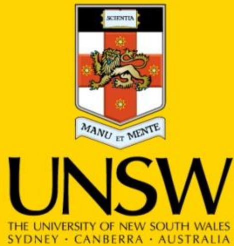

Improved carrier selectivity of diffused silicon wafer solar cells

Never Stand Still

SPREE Seminar

12th October 2017

Alexander To

Supervisor: Dr. Bram Hoex

Co-supervisor: Dr. Alison Lennon

ARENA

Australian Government
Australian Renewable Energy Agency

Improved carrier selectivity

Basic solar cell operation

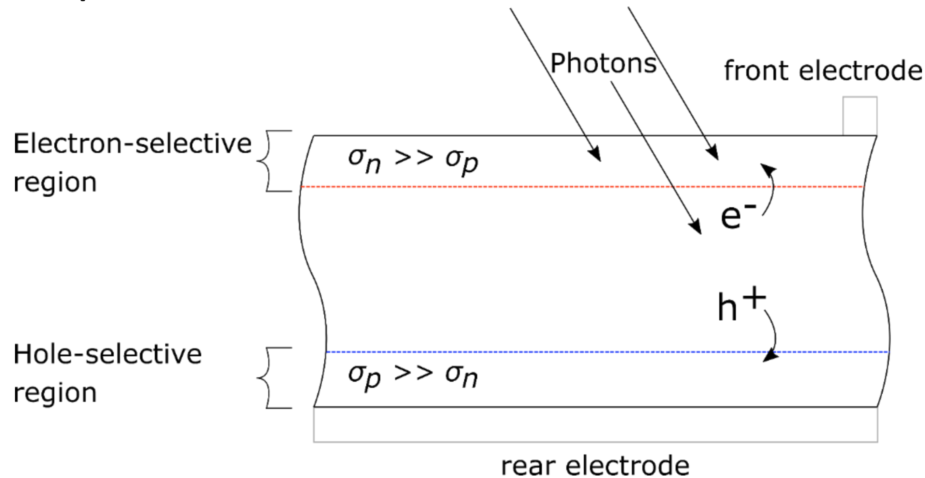

Figure 1 Schematic representation of a basic solar cell, depicting the basic processes occurring in the device which facilitate power conversion and extraction.

Carrier selectivity is engineered to…

1) Reduce recombination, which can quantified by the recombination current density $\boldsymbol{J_0}$.
2) Facilitate the extraction of charge carriers at the metal electrodes, which is measured by the contact resistivity $\boldsymbol{\rho_c}$

Improved Carrier Selectivity

Industry trends/forecasts

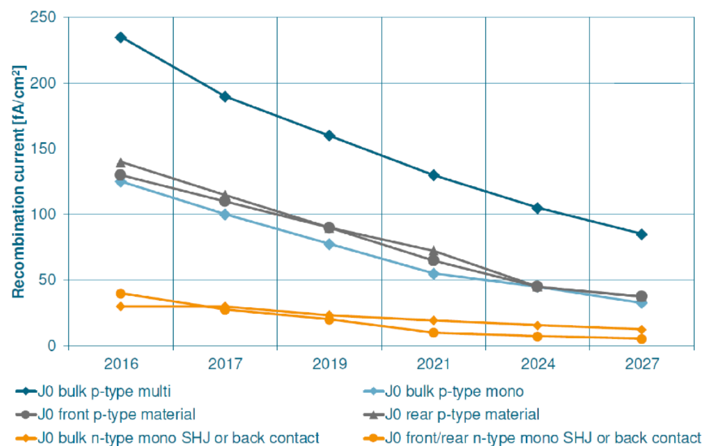

Figure 2 Predicted trend for recombination currents J_{0bulk}, J_{0front}, J_{0rear} for *p*-type and *n*-type solar cell concepts (ITRPV [1])

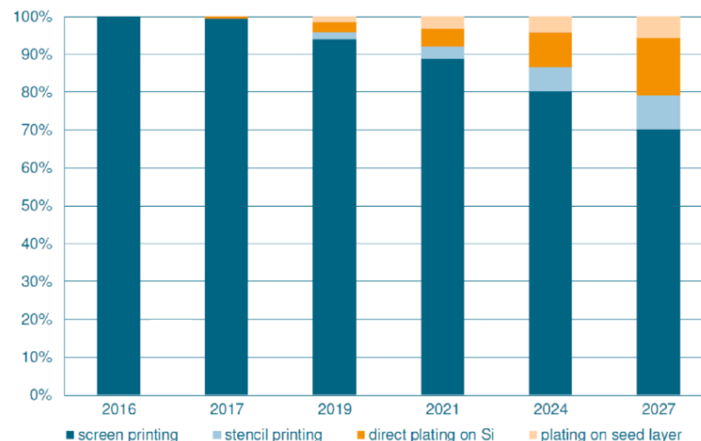

Figure 3 Predicted trend for different front side metallisation technologies, (ITRPV [1])

Thesis aim:

Investigate how the carrier selectivity of diffused solar cells can be improved for the existing and future diffused silicon wafer based solar cell technologies.

[1] *International Roadmap for Photovoltaic Results (ITRPV): Results 2016*. 2017.

Improved carrier selectivity of diffused silicon wafer solar cells

Majority carrier conductivity at p^+ and n^+ metal-silicon interfaces.

1. Exploiting the unintentional consequences of AlO_x wrap around on screen printed n^+ -silicon/Ag contact resistivity.
2. The properties of electroless nickel plated contacts to boron diffused p^+-silicon.

Carrier selectivity at non-contacted diffused surfaces.

3. Understanding the surface recombination rate of diffused and inverted/depleted surfaces.
4. A novel method of extracting the surface recombination parameters from photoconductance measurements.

Applications to diffused homojunction IBC Solar cells

5. Fabrication and simulation solar cells results.

Presentation overview

Improved carrier selectivity of diffused silicon wafer solar cells

Majority carrier conductivity at p^+ and n^+ metal-silicon interfaces.

1. Exploiting the unintentional consequences of AlO_x wrap around on screen printed n^+ -silicon/Ag contact resistivity.
2. The properties of electroless nickel plated contacts to boron diffused p^+-silicon.

Characterising carrier selectivity at non-contacted diffused surfaces.

3. Understanding the surface recombination rate of diffused and inverted/depleted surfaces.
4. A novel method of extracting the surface recombination parameters from photoconductance measurements.

Applications to diffused homojunction IBC Solar cells

5. Fabrication and simulation solar cells results.

ARC Photovoltaics Centre of Excellence UNSW
UNSW THE UNIVERSITY OF NEW SOUTH WALES SYDNEY · CANBERRA · AUSTRALIA

The effect of AlO_x wrap-around

Overview

- In principle, single sided deposition is actually very hard to achieve and parasitic deposition onto the front side of the solar cell can occur during fabrication.
- This has been reported for both PECVD and ALD AlO_x deposition processes.

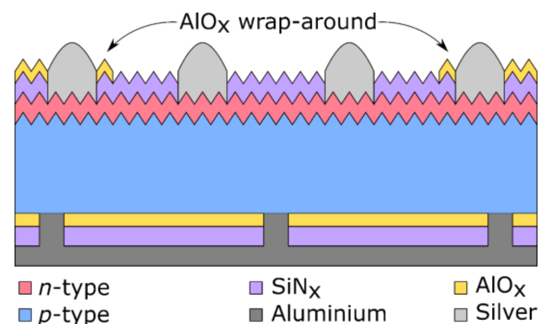

Figure 4 Schematic of a *p*-PERC solar cell with AlO_x wrap-around on the front surface edges studied in this work..

Research questions:

1) What is the effect of AlO_x wrap-around on screen-printed contact resistance?
2) Can we model this effect on solar cell performance?
3) What is the effect of AlO_x wrap on *p*-PERC solar cell performance?

The effect of AlO_x wrap-around

Methodology:

1. Fabricate TLM test structures with intervening AlO_x layers.

   Vary: Paste, Temperature, Speed.

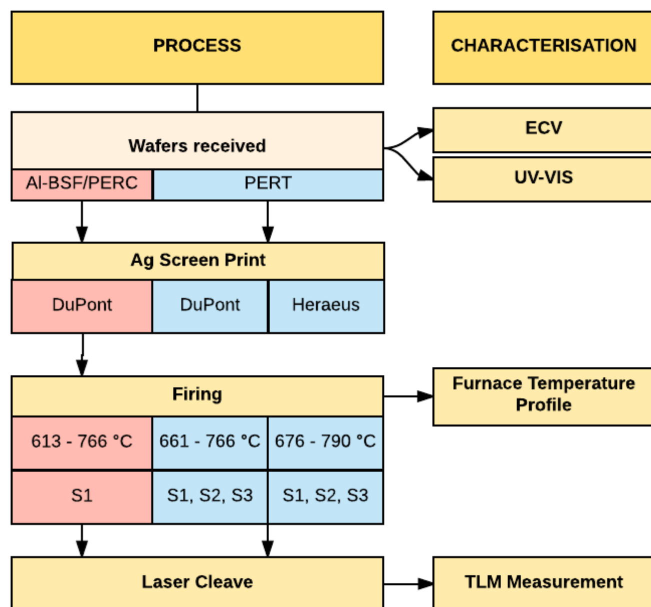

Figure 5 Processing sequence of the PERC and PERT precursors.

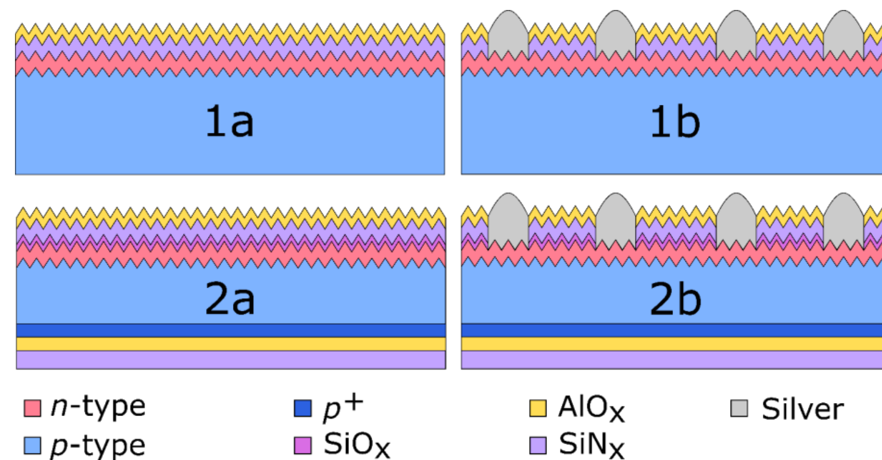

Figure 6 Schematic diagram of the *p*-type PERC (top) and PERT (bottom) test structures used in this experiment.

ARC Photovoltaics Centre of Excellence UNSW

UNSW THE UNIVERSITY OF NEW SOUTH WALES SYDNEY · CANBERRA · AUSTRALIA

The effect of AlO_x wrap-around

Methodology:

1. Fabricate TLM test structures.

Vary: Paste, Temperature, Speed.

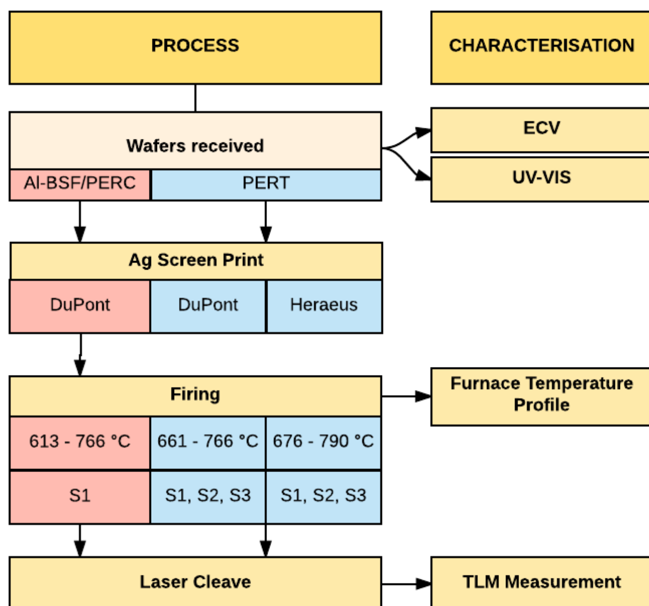

Figure 7 Processing sequence of the PERC and PERT precursors.

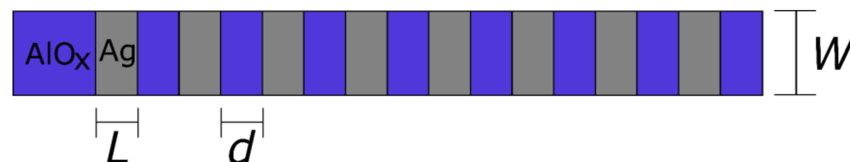

Figure 4 Top view of the equidistant linear TLM structure.

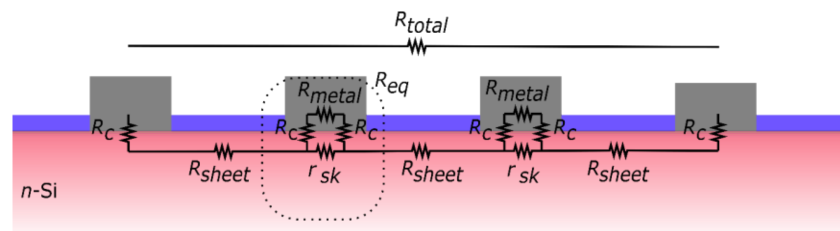

Figure 8 Equivalent resistance network for a system of with two interjacent fingers.

$$R_{total} = (n+1)\frac{R_{sheet}d}{W} + 2R_c + \boldsymbol{nR_{eq}}$$

$$R_{eq} = \left(\frac{1}{r_{sk}} + \frac{1}{2R_c + R_{metal}}\right)^{-1}$$

ARC Photovoltaics Centre of Excellence UNSW
UNSW THE UNIVERSITY OF NEW SOUTH WALES SYDNEY · CANBERRA · AUSTRALIA

The effect of AlO_x wrap-around

Contact resistivity ρ_c – PERC Structures.

Key points:

1) A clear ‘U’-shaped trend, representing a minimum firing temperature.
2) 3 and 5 nm thicknesses appear to improve ρ_c
3) A thick (10 nm) AlO_x layer adversely affects ρ_c

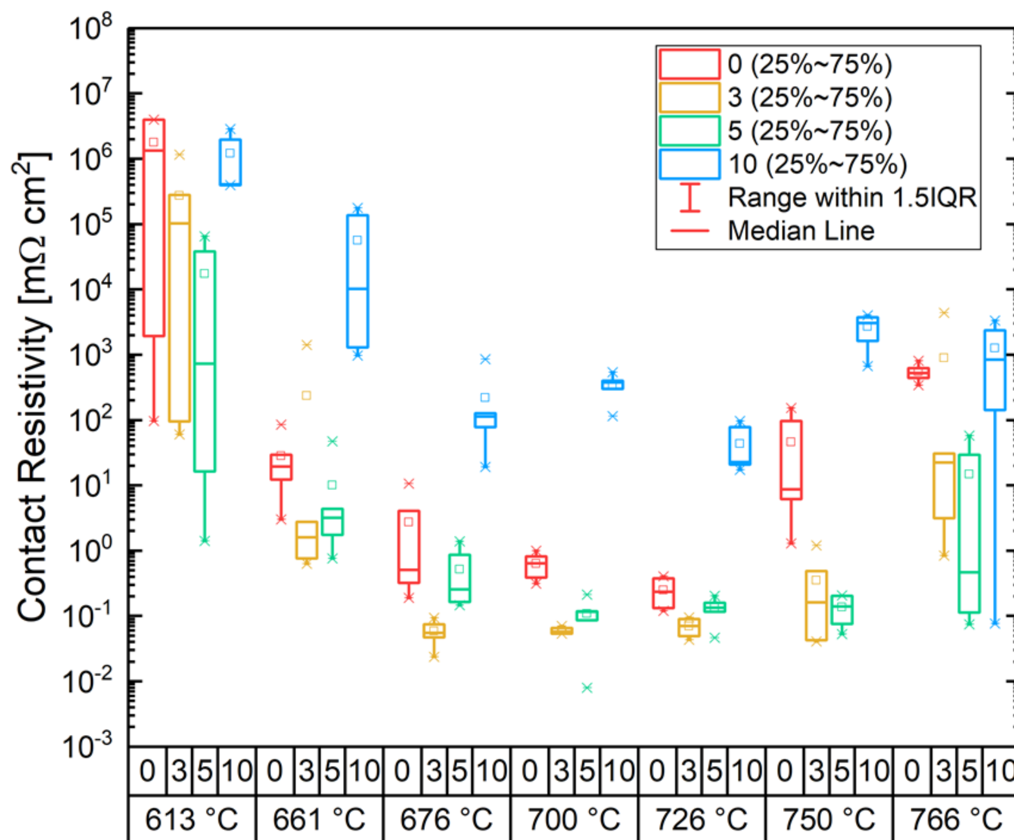

Figure 9 Contact resistivity vs. temperature for screen-printed silver fingers fired through an AlO_x/SiN_x stack.

To, A. et. al., *IEEE JPV* (2017) **99** p. 1-8

Research The effect of AlO_x wrap-around

Contact resistivity ρ_c – PERT Structures, varying paste.

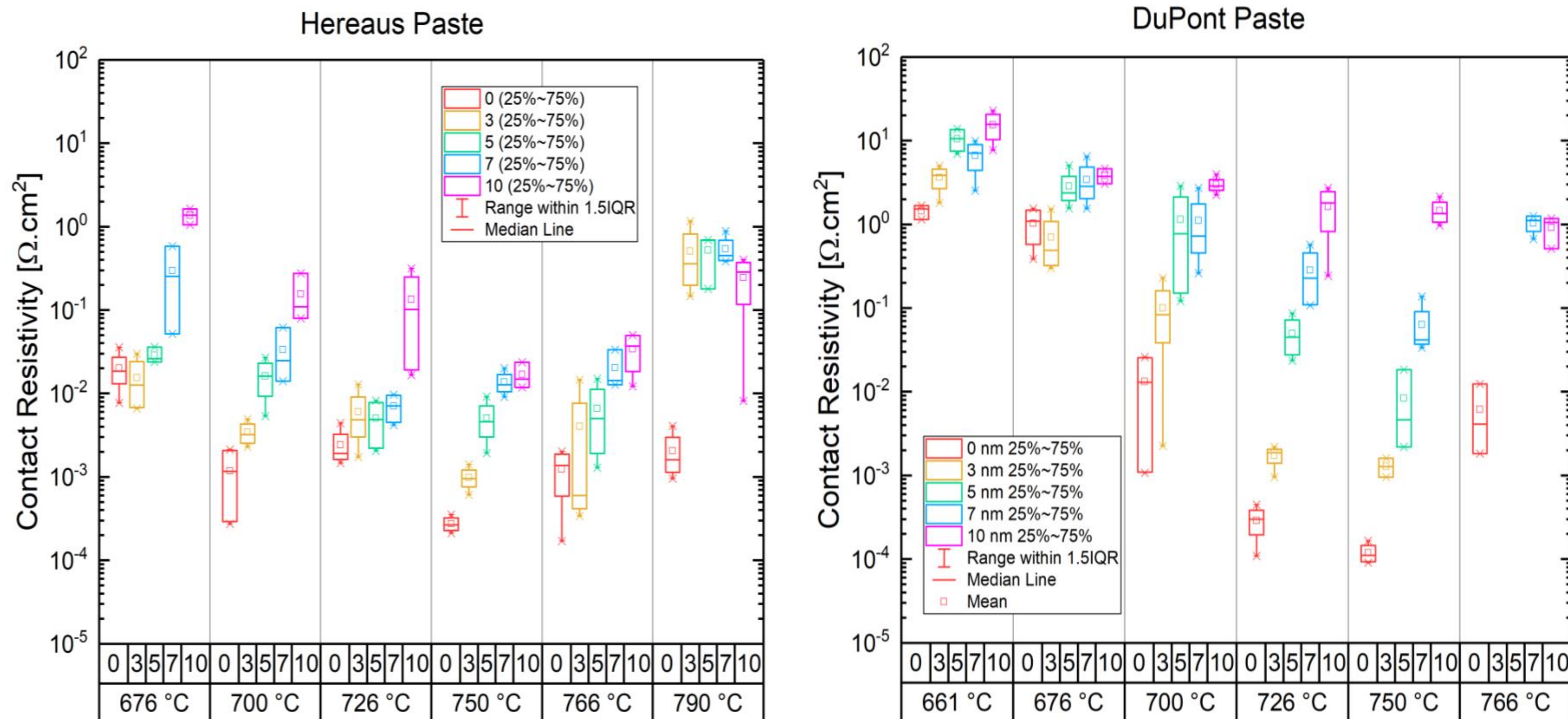

Figure 10 Contact resistivity vs. firing temperature for Ag-Si contacts formed with Hereaus (left) and DuPont (right) paste on PERT precursor wafers, for various AlO_x thicknesses.

The effect of AlO_x wrap-around

Contact resistivity ρ_c – PERT Structures, varying speed.

Key points:

1) Varying speed does not appear to have significantly improved the
2) The Hereaus paste tested tends to perform better than the Dupont paste tested.

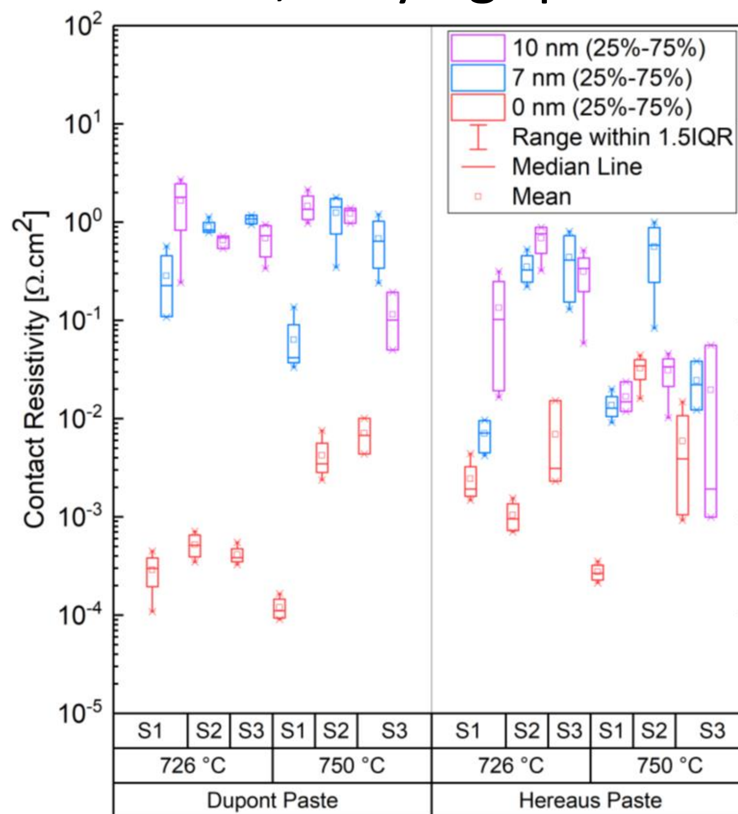

Figure 11 Contact resistivity for PERT precursor samples fired at belt speeds S1, S2 and S3 using both Heraeus and DuPont silver pastes, with AlO_x capping thicknesses ranging between 0–10 nm.

Contact resistivity ρ_c error analysis.

- **Scenario 1:** Negligible current flows through the doped region under the metal (Low R_c)

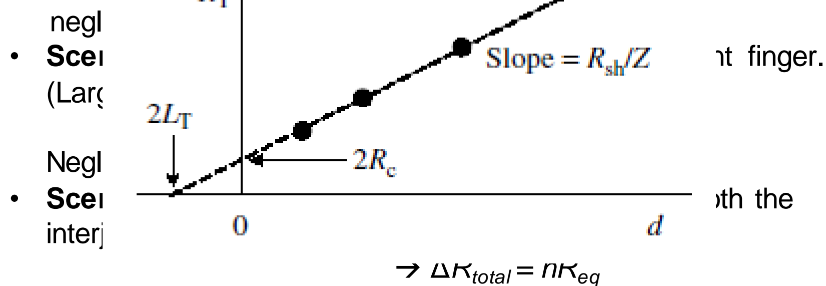

negl
- **Scen**... nt finger.
(Larg

Negl
- **Scen**... oth the
interj

$\rightarrow \Delta R_{total} = nR_{eq}$

which will introduce non-negligible error for high R_c, and r_{sk}.

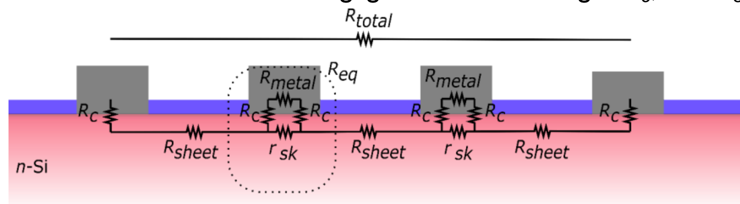

Figure 8 Equivalent resistance network for a system of with two interjacent fingers.

$$R_{total} = (n+1)\frac{R_{sheet}d}{W} + 2R_c + \boldsymbol{nR_{eq}}$$

$$R_{eq} = \left(\frac{1}{r_{sk}} + \frac{1}{2R_c + R_{metal}}\right)^{-1}$$

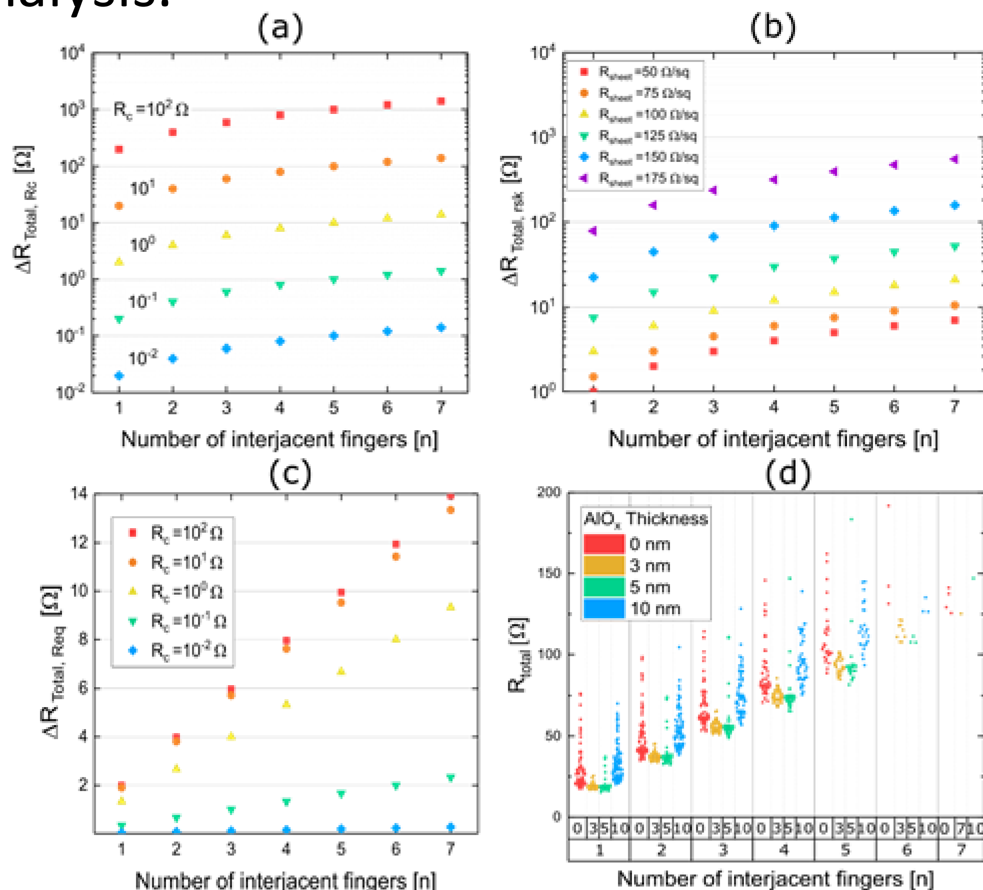

Figure 12 Absolute error ΔR_{total} for the Scenarios 1, 2 and 3, is represented in (a), (b) and (c), respectively, with (d) showing the measured R_{total} as a function of n for all samples and AlO_x thicknesses.

To, A. et. al., *E. Procedia* (2017) **124** p. 914-921
Schroder, *Semiconductor material and device characterization* (2006) Wiley & Sons 3rd Edition.

2. Modelling the effect of wrap-around using Griddler

Methodology:

1. Simulate a state-of-the-art *p*-PERC solar cell in Griddler using published simulation values.
2. Impose ρ_c non-uniformity spatially and simulate solar cell performance for various AlO_x thicknesses and wrap-around extents.

Table 1 Griddler simulated performance characteristics of a *p*-PERC solar cell without AlO_x wrap-around.

Symbol	Parameter	Value
η	Efficiency	21.31 %
V_{oc}	Open circuit voltage	662 mV
J_{sc}	Short circuit current density	39.87 mA.cm^{-2}
FF	Fill factor	80.77 %

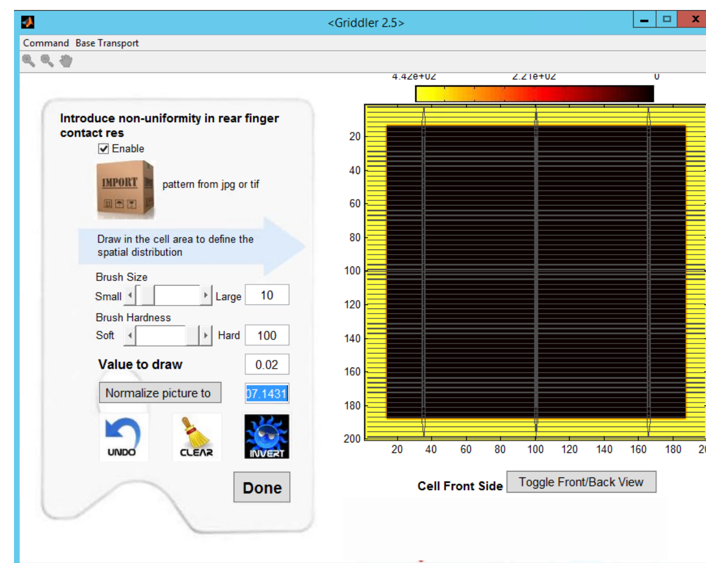

Figure 13 Screenshot of the Griddler interface in which spatial non-uniformity is simulated.

The effect of AlO_x wrap-around

Modelling Results

1) A 3 and 5 nm AlO_x does not improve state-of-the-art cells which are not ρ_c limited.
2) A thickness of 10 nm can have a significant effect on cell *FF*.

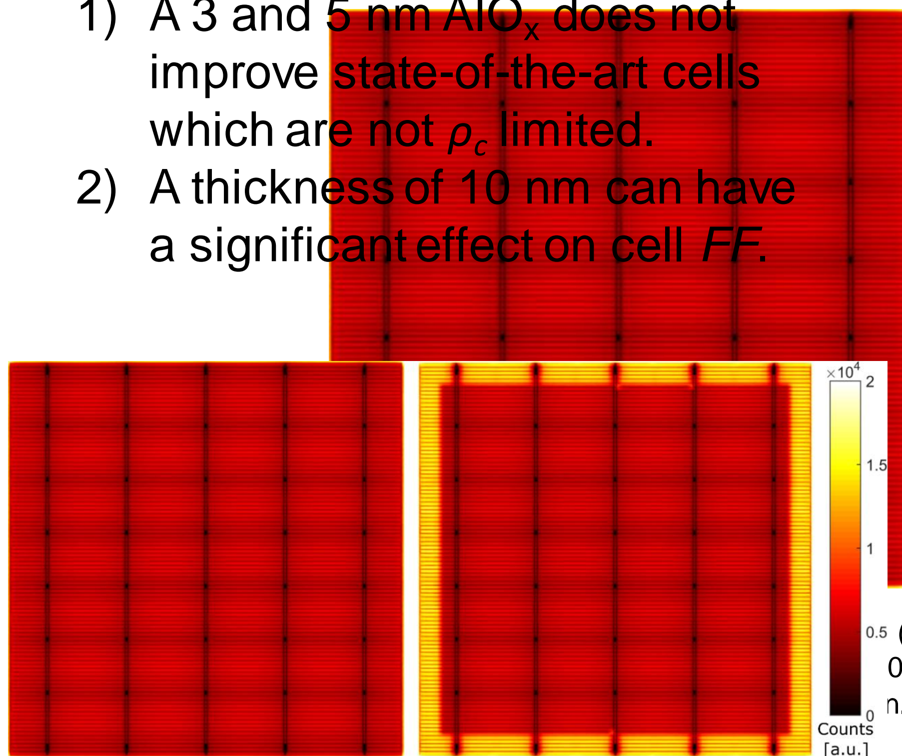

Figure 14 Simulated PL images (at V_{mpp} with current extraction) of a *p*-PERC solar cell with (left) 0 and (right) 10 mm of 10 nm thick AlO_x wrap-around deposition.

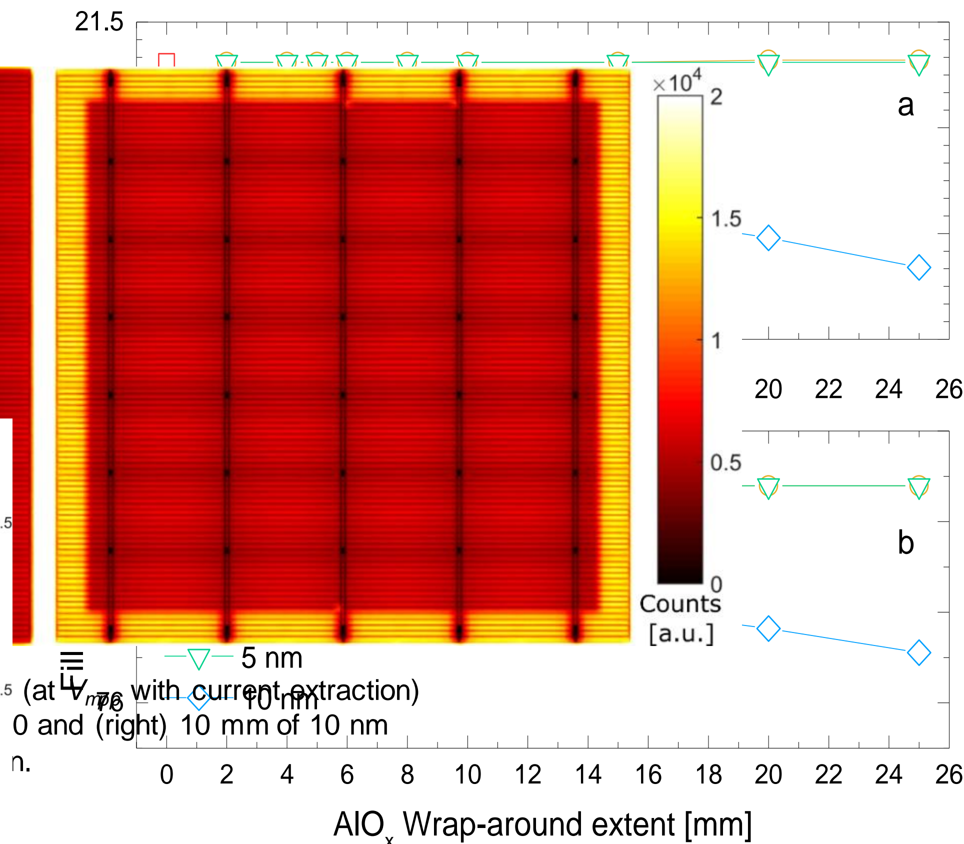

Figure 15 Simulated effect of parasitic front side AlO_x deposition on: (a) efficiency; and (b) *FF*, of a *p*-PERC solar cell.

To, A. et. al., *IEEE JPV* (2017) **99** p. 1-8

ARC Photovoltaics Centre of Excellence UNSW
UNSW THE UNIVERSITY OF NEW SOUTH WALES SYDNEY · CANBERRA · AUSTRALIA

The effect of AlO_x wrap-around

3. Effect actual solar cell performance

Methodology:

1. Fabricate *p*-type Al-BSF solar cells with an SiN_x/AlO_x stack, of varying AlO_x thicknesses.
2. Reduce $N_{D, surface} = 3x10^{19}$ cm^{-3}

Characterisation:

1. Light/Dark-IV
2. Suns-V_{oc}
3. Calculate R_{series}:

$$R_{series} = \frac{V_{mp,SunsVoc} - V_{mp,LIV}}{J_{mp,light}}$$

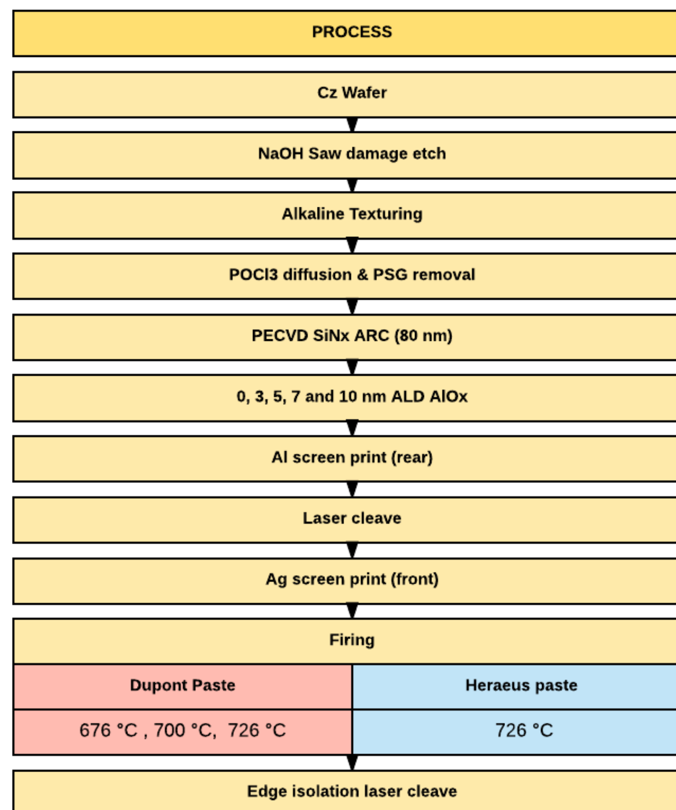

Figure 16 Processing sequence for the *p*-type Al-BSF cells fabricated in this work.

To, A. et. al., *IEEE JPV* (2017) **99** p. 1-8

The effect of AlO_x wrap-around

3. Effect of wrap around on solar cell performance

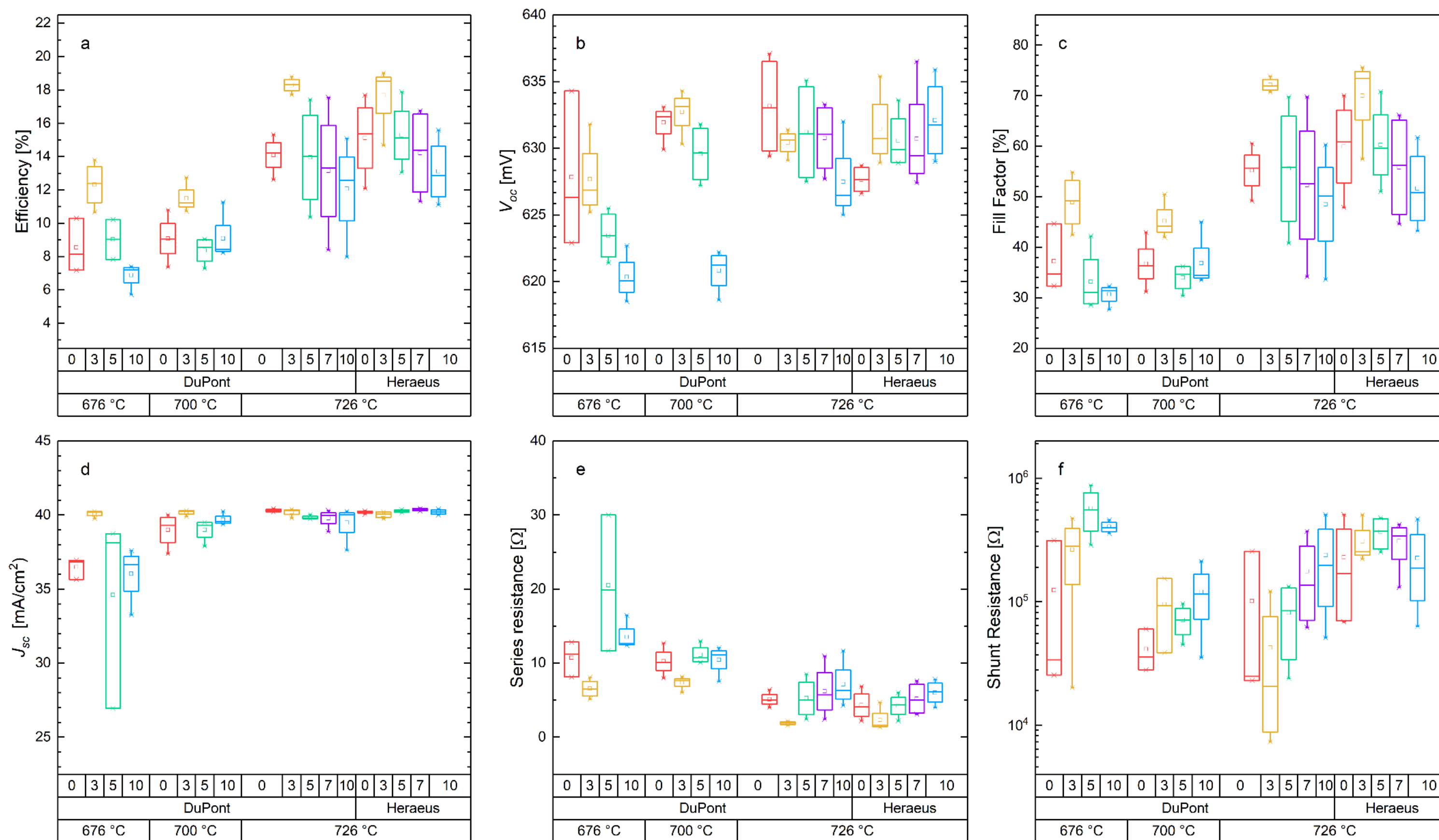

Figure 17 Cell characteristics extracted from light-*IV*, dark-*IV* and Suns-V_{OC} measurements for Al-BSF solar cells screen-printed with DuPont and Heraeus paste at varying peak temperatures.

To, A. et. al., *IEEE JPV* (2017) **99** p. 1-8

The effect of AlO_x wrap-around

3. Effect of wrap around on solar cell performance

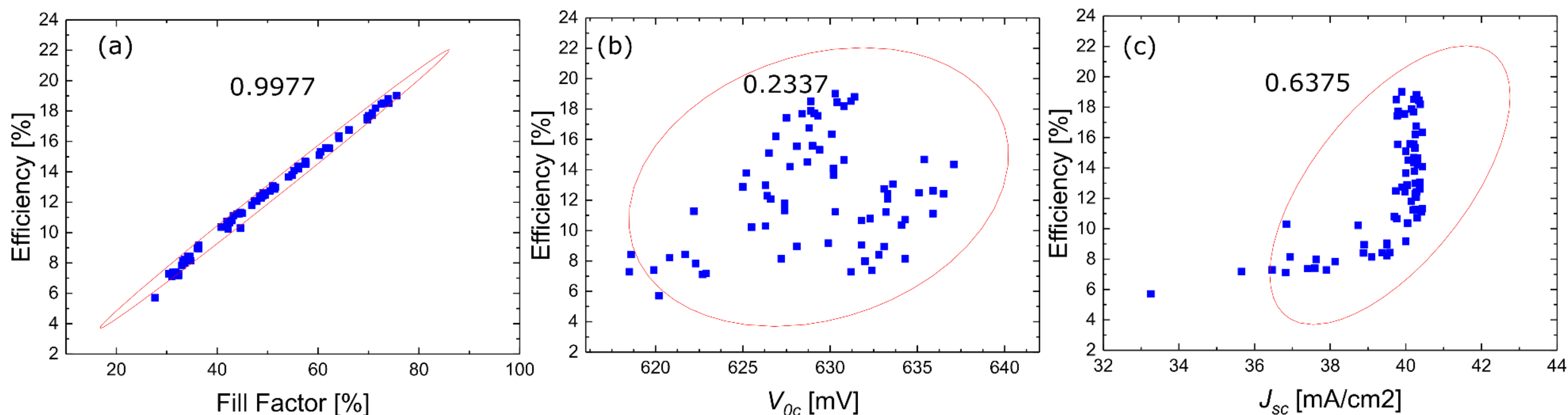

Figure 18 Plots of correlations between *Efficiency* (a), V_{oc} (b) and J_{sc} (c) vs. efficiency.

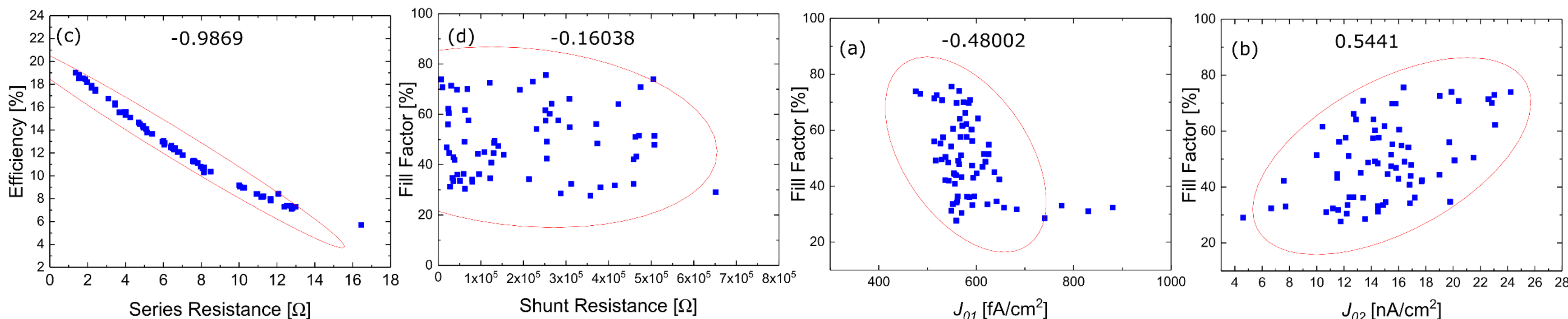

Figure 19 Plots of correlations between J_{01} (a), J_{02} (b) and series resistance(c) and shunt resistance (d) vs. efficiency

ARC Photovoltaics Centre of Excellence UNSW
UNSW THE UNIVERSITY OF NEW SOUTH WALES SYDNEY · CANBERRA · AUSTRALIA

The effect of AlO_x wrap-around

Summary:

1) The thickness of AlOx wrap-around has a significant effect on contact resistivity during firing:
    1) 3 and 5 nm thick AlO_x layers were shown to reduce ρ_c.
    2) 7 and 10 nm layers were shown to increase ρ_c.
    3) The paste composition can significantly affect ρ_c for a given firing condition.
    4) Varying speed was not able to improve ρ_c for thicker layers.
2) Griddler can be used to effectively simulate non-spatial uniformities in contact resistivity.
3) Solar cells fabricated with reduced surface concentration were fabricated:
    1) 3 nm AlO_x layers were better able to contact the low doped phosphorous electron collector.
    2) 5 nm layers had higher variability relative to the control, 7 and 10 nm layers had poor performance.

ARC Photovoltaics Centre of Excellence UNSW
UNSW THE UNIVERSITY OF NEW SOUTH WALES SYDNEY · CANBERRA · AUSTRALIA

Presentation overview

Improved carrier selectivity of diffused silicon wafer solar cells

Majority carrier conductivity at p^+ and n^+ metal-silicon interfaces.

1. Exploiting the unintentional consequences of AlO_x wrap around on screen printed n^+ -silicon/Ag contact resistivity.
2. The properties of electroless nickel plated contacts to boron diffused p^+-silicon.

Characterising carrier selectivity at non-contacted diffused surfaces.

3. Understanding the surface recombination rate of diffused and inverted/depleted surfaces.
4. A novel method of extracting the surface recombination parameters from photoconductance measurements.

Applications to diffused homojunction IBC Solar cells

5. Fabrication and simulation solar cells results.

Electroless nickel plated contacts

Why electroless nickel plated contacts to diffused *p*-type silicon?

1. Growing (albeit small) market share of *n*-type solar cells require contact to p^+ emitter.
2. Broader benefits of plating – self aligned, potentially low costs, higher aspect ratio relative to screen printing. Avoids problems with Al-spiking the emitter.
3. Processing advantages of plating both *n*-type and *p*-type layers in bifacial solar cells in one step (no prior metal contacts required).

Research questions:

1) What are the electrical properties of electroless nickel plated contacts? metrics:
    1) Contact saturation current (J_{0c})
    2) Contact specific resistivity (ρ_c)
2) How are these properties affected by the diffusion profile?
    1) Surface concentration of dopants ($N_{A,s}$)
    2) Dopant depth (x_d)
3) How do these trends and properties compare with other metallisation technologies?
    1) Aluminium evaporated vs. Nickel plated contacts.

Electroless Nickel Plated Contacts

Approach: 1. Development of a nickel plating process.

Basic reaction:

$$\mathbf{M^{z+}_{solution} + Red_{solution} \xrightarrow{\text{catalytic surface}} M_{solid} + Ox_{solution}}$$

1) With activation:

A palladium-tin colloid is used to sensitise the silicon surface to act as catalysing sites for the Ni deposition.

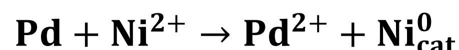

$$\mathbf{Pd + Ni^{2+} \rightarrow Pd^{2+} + Ni^{0}_{cat}}$$

2) Without Activation:

No prior sensitisation required. Two mechanisms:

1) Surface reduction a result of reducing agent ($2H_2PO_2$) and/or

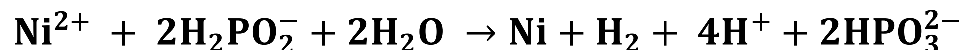

$$\mathbf{Ni^{2+} + 2H_2PO_2^- + 2H_2O \rightarrow Ni + H_2 + 4H^+ + 2HPO_3^{2-}}$$

2) Galvanic displacement reaction

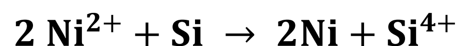

$$\mathbf{2\,Ni^{2+} + Si \rightarrow 2Ni + Si^{4+}}$$

Electroless Nickel Plated Contacts

Approach: 1. Development of a nickel plating process.

Process:

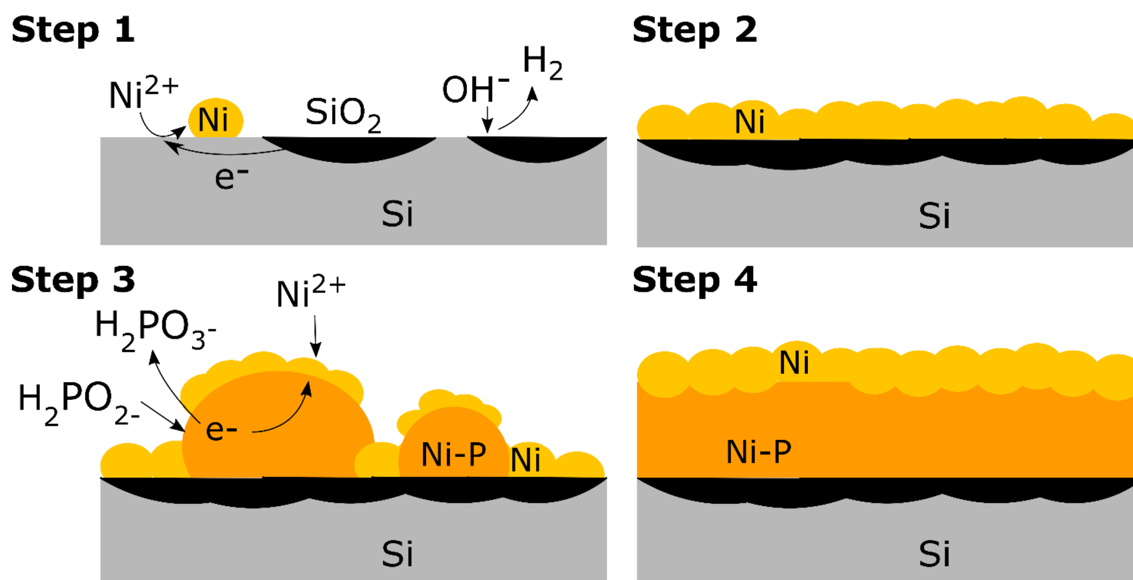

Figure 21 The nucleation and growth of electroless nickel plated layers in electrolytes with a hypophosphite reducing agent.

Electroless Nickel Plated Contacts

Approach: 1. Development of a nickel plating process.

Process:

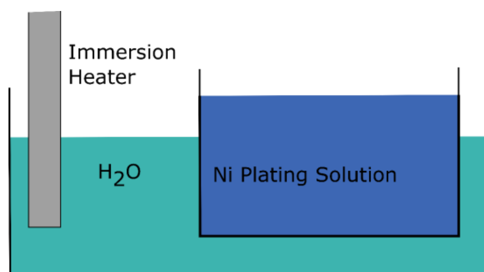

Figure 22 A schematic of the experimental apparatus used for the ENP performed in this study.

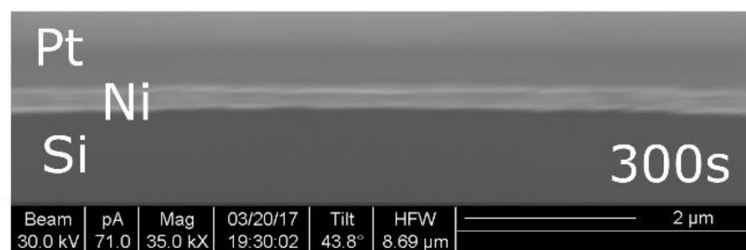

Figure 23 SEM images of the focused-ion-beam milled cross-sectional interface of the ENP layer.

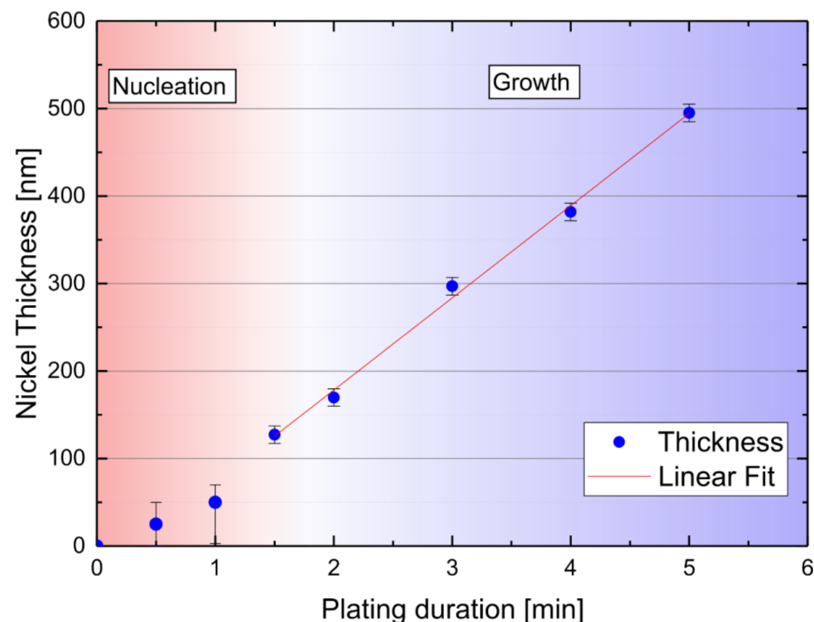

Figure 24 Measured average nickel thickness vs. immersion duration in an alkaline ENP electrolyte with a pH = 10.2 and T = 52 °C. The growth rate was found to be 1.76 nm/s.

ARC Photovoltaics Centre of Excellence UNSW
UNSW THE UNIVERSITY OF NEW SOUTH WALES SYDNEY · CANBERRA · AUSTRALIA

Electroless Nickel Plated Contacts

Approach: 2. Development of a boron diffusion process

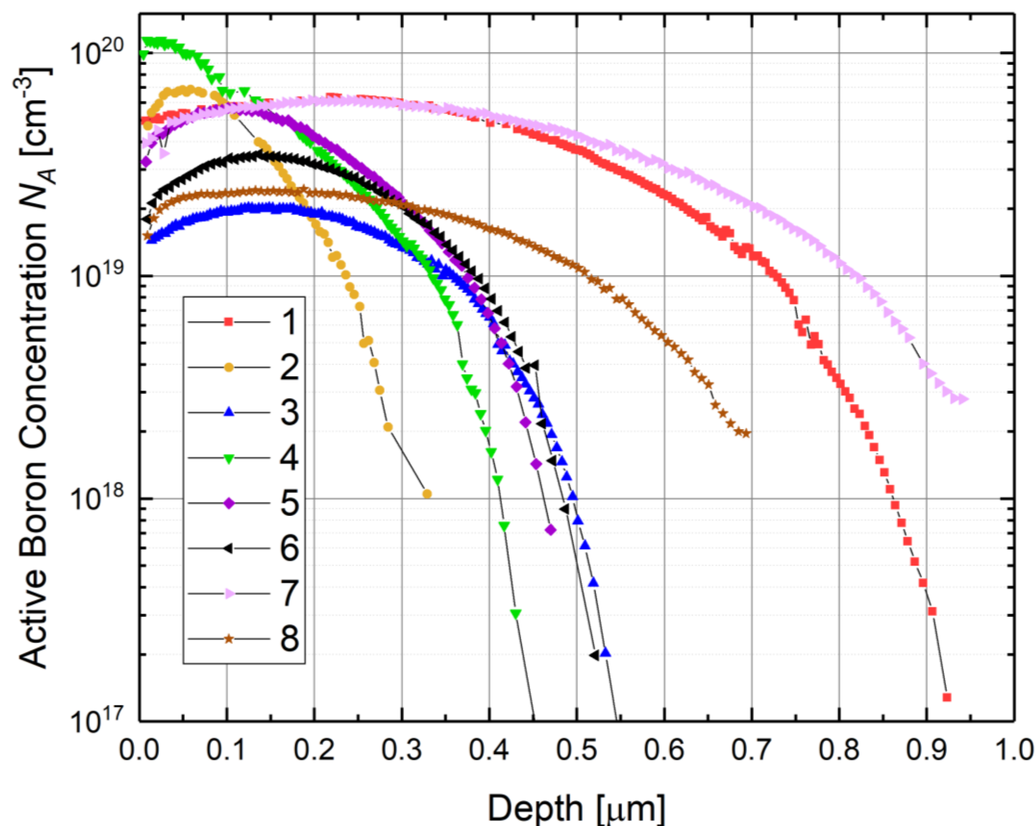

Figure 25 ECV profiles of the electrically-active boron concentration as a function of depth from the surface for the different boron diffusion recipes used in this study.

Recipe ID	Average Sheet Resistance[a] R_{sheet} [Ω/□]	Surface conc.[b] $N_{A,s}$ [cm^{-3}]	Peak conc.[b] N_p [cm^{-3}]	Junction depth[b] x_j [μm]
1	41	4.95×10^{19}	6.10×10^{19}	1.0
2	110	4.70×10^{19}	6.85×10^{19}	0.31
3	140	1.40×10^{19}	2.12×10^{19}	0.59
4	63	9.90×10^{19}	1.14×10^{20}	0.51
5	76	3.25×10^{19}	5.67×10^{19}	0.48
6	100	1.8×10^{19}	3.51×10^{19}	0.52
7	31	3.94×10^{19}	6.14×10^{19}	0.95
8	89.2	1.51×10^{19}	2.45×10^{19}	0.69

Approach: 3. Extraction of J_{0c} and ρ_c.

1. Contact resistivity extraction:
   1. via Circular TLM (without activation) linear TLM (with Pd/Sn activation).
2. Contact recombination J_{0c} extraction:

   Calibrated PL measurements[1].
   1. Sample calibration (Thickness, ECV, Sheet res, PC lifetime, UV-Vis, bulk resistivity, PL measurement, Bulk lifetime).
   2. Simulation of PL in the unprocessed region in Quokka.
   3. Calculation of calibration factor A

$$A = \frac{\textit{measured PL counts}}{\textit{simulated PL counts}}$$

   4. Measurement of the average PL counts in the processed region.
   5. Calculation of target PL counts in simulation.
   6. Simulation of PL counts, fitted to target PL counts, with J0c as free parameter.

[1]Fell, A. *Energy Proc.*, **38**, 22-31, (2013)

Electroless Nickel Plated Contacts

Approach: 4. Fabrication and structures

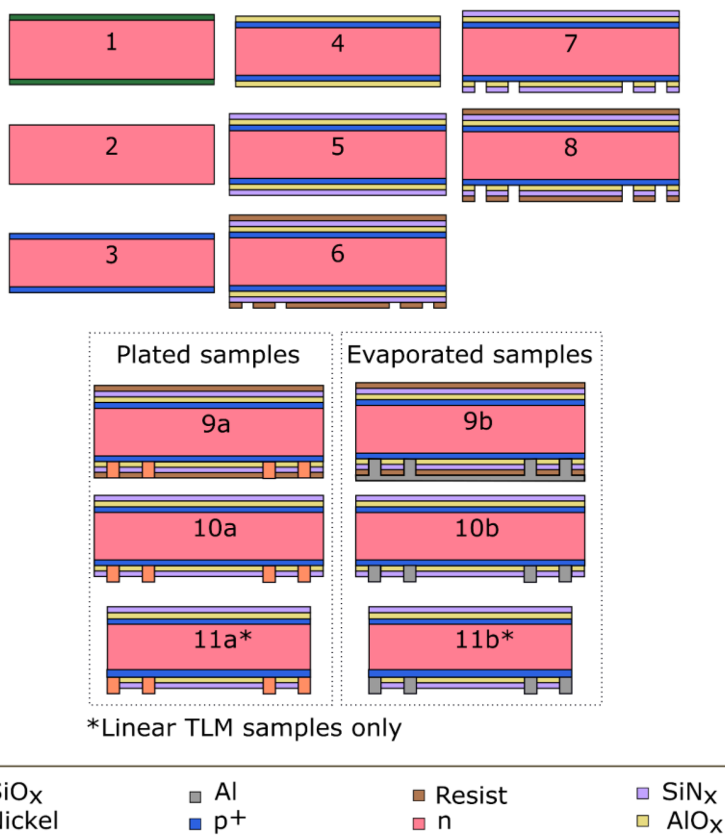

Figure 26 Processing sequence for all wafers used in this work.

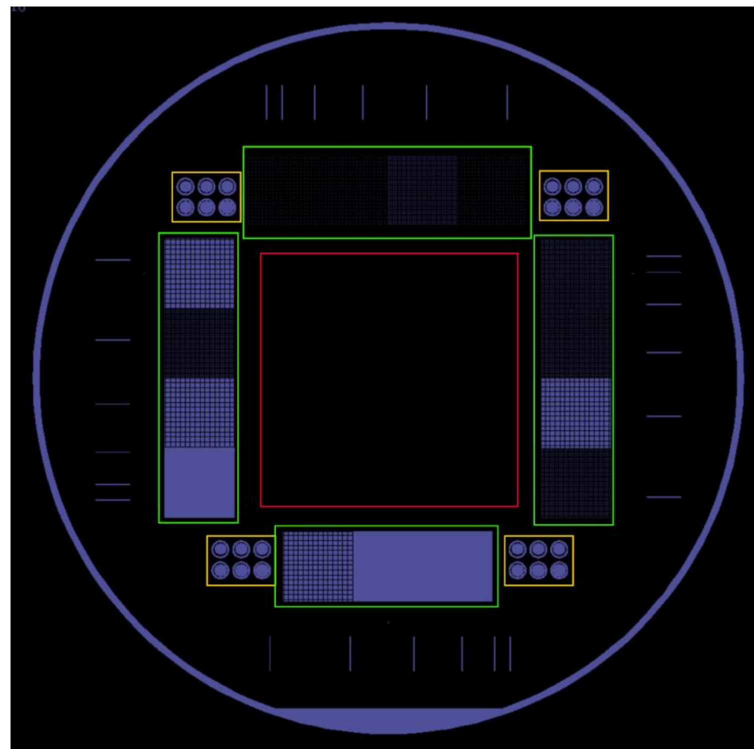

Figure 27 Schematic drawing of the 100 mm mask used to define the circular TLM patterns (yellow boxes), a series of 15 contact recombination arrays (green boxes), and a central region for PC lifetime measurement (red box).

[1]Fell, A. *Energy Proc.*, **38**, 22-31, (2013)

ARC Photovoltaics Centre of Excellence UNSW
UNSW THE UNIVERSITY OF NEW SOUTH WALES SYDNEY · CANBERRA · AUSTRALIA

Electroless Nickel Plated Contacts

Contact resistivity ρ_c

Key Points:

1) No clear trend of ρ_c vs. $N_{A,s}$ for plated samples.
2) $\rho_{c\,Ni} >> \rho_{c\,Al}$
3) Process is not consistent

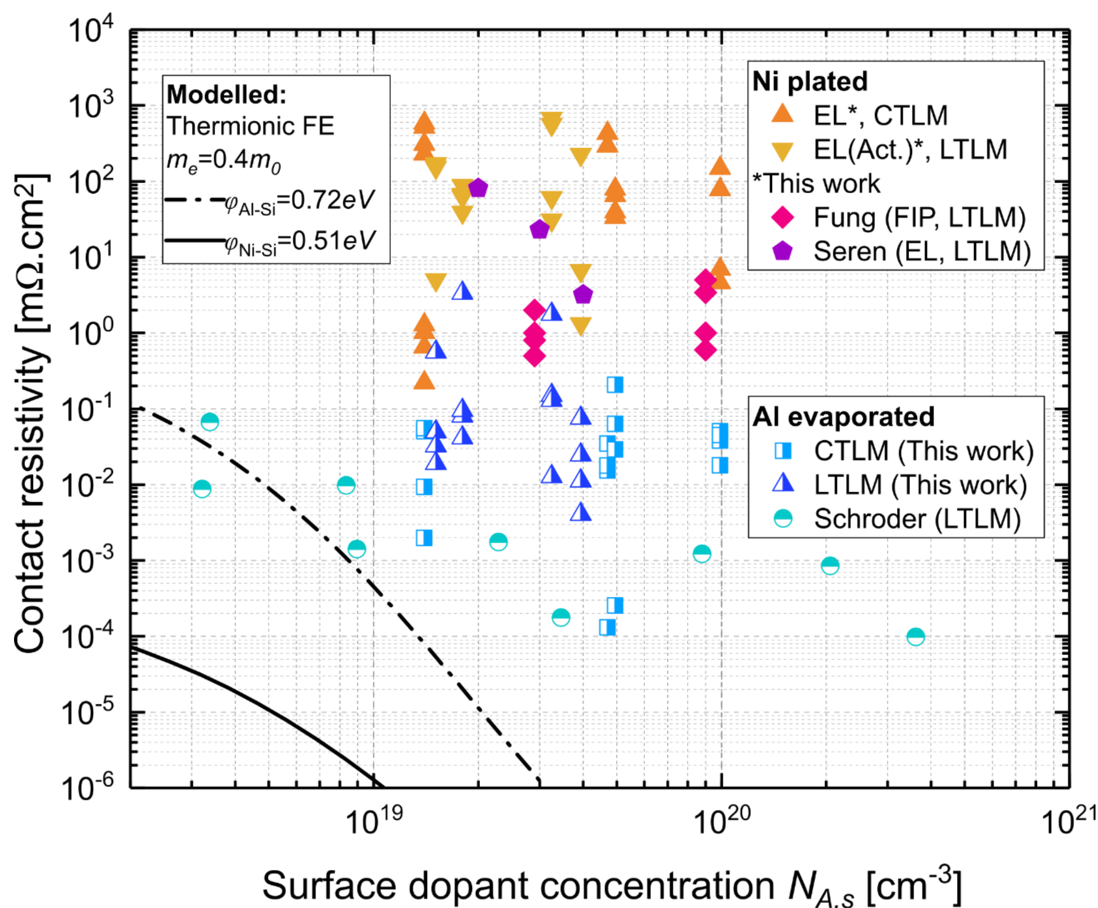

Figure 28 Compilation of measured ρ_c values resulting from aluminium evaporated and nickel plated contacts formed on heavily diffused *p*-type silicon. Solid and dashed lines indicate modelled thermionic field emission ρ_c values.

Schroder, D.K., Semiconductor Mat. & Dev. Char., (2006) p.127-184.

Contact resistivity – discussion

1) Process is difficult, hard to reproduce.
2) Presence of interfacial oxide layer is likely to affect contact resistivity for plated samples.

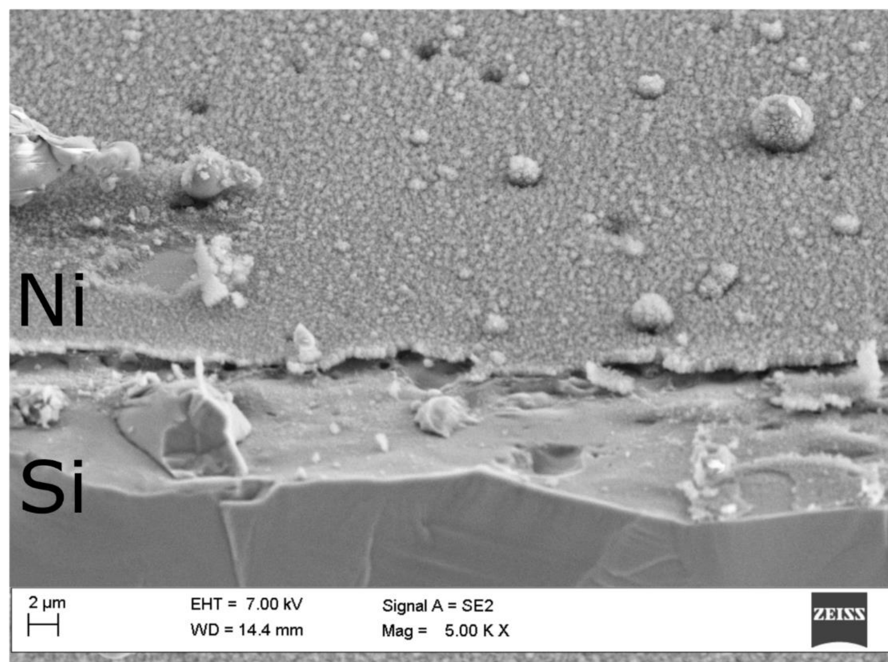

Figure 29 SEM images of the nickel plated silicon surface (a) after annealing at 350 °C, and with close up view of the large deposits (b) which are non-uniformly distributed across the entire surface.

Contact recombination – effect of contact fraction

Key Points:

1) J_{0c} plated > J_{0c} evaporated.
2) For each contact fraction, a range of J_{0c} values can be attained.
3) No statistically significant trend with contact fraction vs J_{0c}.

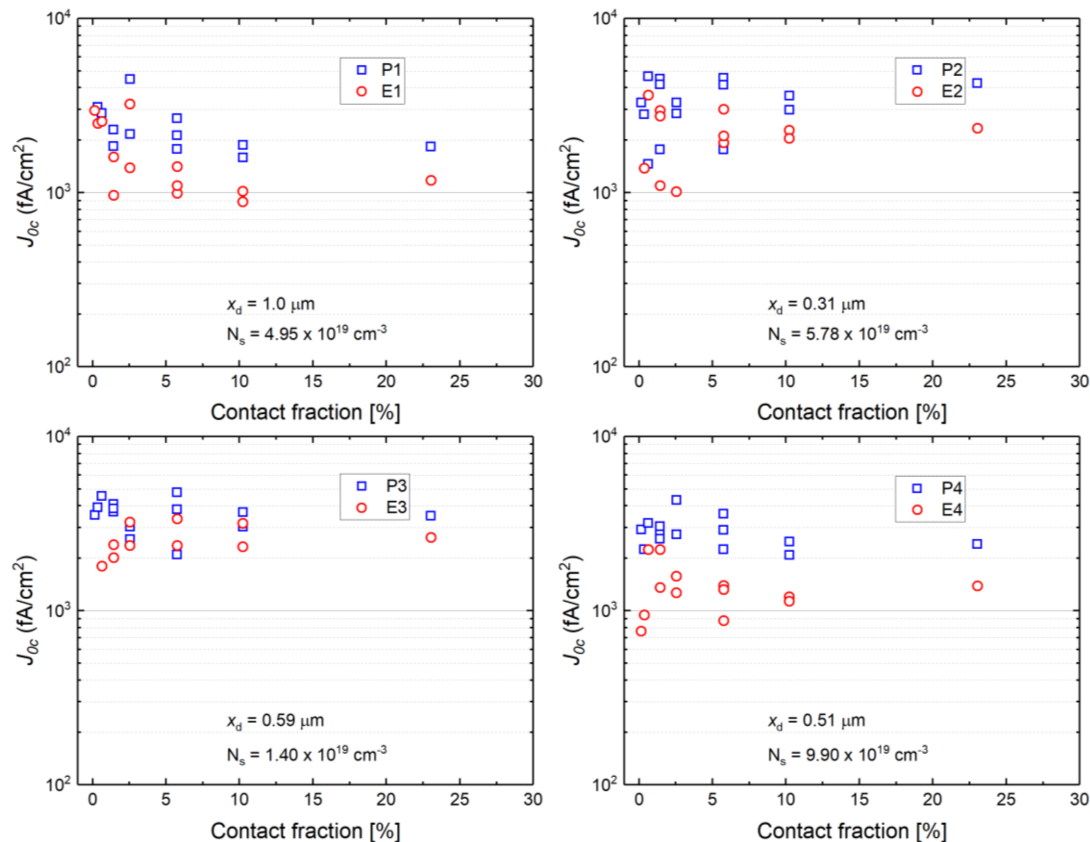

Figure 30 Estimated J_{0c} graphed as a function of contact fraction for each diffusion recipe.

ARC Photovoltaics Centre of Excellence UNSW
UNSW THE UNIVERSITY OF NEW SOUTH WALES SYDNEY · CANBERRA · AUSTRALIA

Contact recombination – effect of junction depth

Key Points:

1) As N_{As} increases, J_{0c} decreases (plots a and c, P/E3 and P/E4).
2) As junction depth increases, J_{0c} decreases. (plot P/E1 and P/E2, plot B only.)

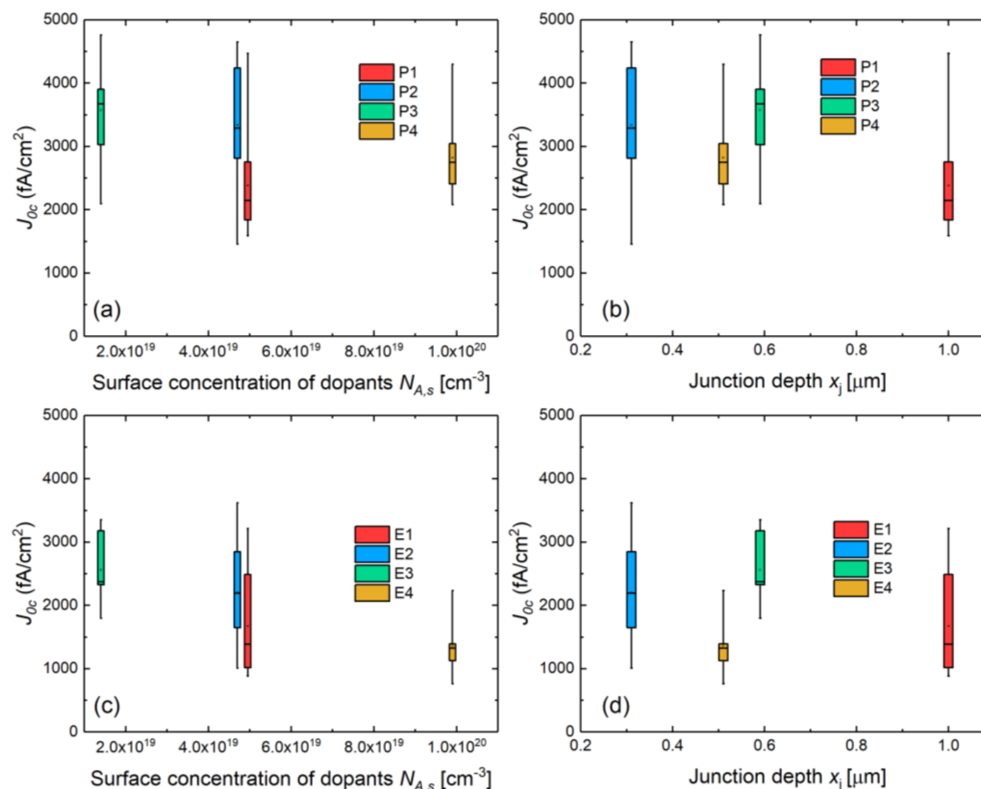

Figure 31 Estimated J_{0c} as a function of active surface dopant concentration and junction depth for plated (top row) and evaporated samples (bottom row).

ARC Photovoltaics Centre of Excellence UNSW

UNSW THE UNIVERSITY OF NEW SOUTH WALES SYDNEY · CANBERRA · AUSTRALIA

Contact recombination – discussion

Sources of variance:
1) Sample non-uniformity.
2) Pixel resolution of PL camera.
3) Sensitivity of the bulk lifetime
4) Optical Absorption at rear.

Reasons for J_{0c} plated > J_{0c} evaporated.
1) Surface roughening.
2) Lattice distortion
3) Etching of silicon surface
4) Surface contamination.

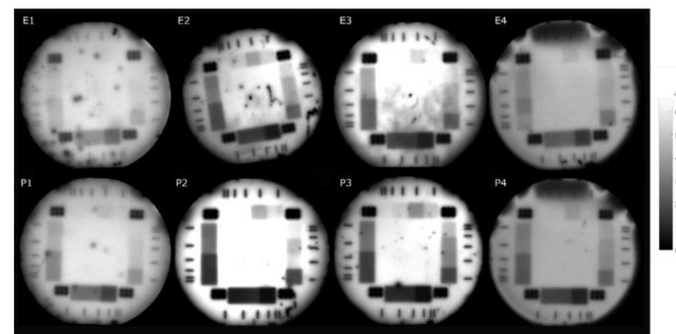

Figure 32 PL images of all samples depicting good uniformity for all samples except E2 and E3.

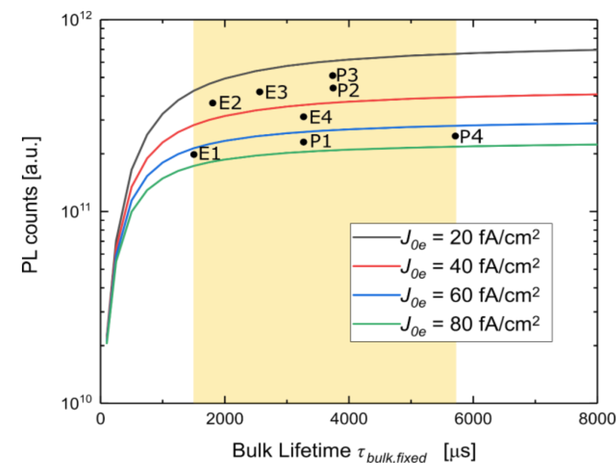

Figure 33 Quokka simulated PL counts for the unprocessed region as a function of Tau_bulk and J_{0e}.

ARC Photovoltaics Centre of Excellence UNSW
UNSW THE UNIVERSITY OF NEW SOUTH WALES SYDNEY · CANBERRA · AUSTRALIA

Electroless Nickel Plated Contacts

Summary:

1) An electroless nickel process was developed and the contact properties assessed relative to evaporated aluminium contacts.
2) Electroless nickel plated contacts are capable of low resistivity ($\rho_{c,average}$ < 1 mΩ.cm^{-2}) contacts to p^+ surfaces, although:
    1) The aluminium evaporated contacts provide lower values and
    2) There are issues with process repeatability.
3) The diffusion profile has an impact on the electrical properties J_{0c} and ρ_c
    1) Higher N_{As} = Lower J_{0c}
    2) Deeper x_j = Lower J_{0c}
4) More interface analysis required to:
    1) Ascertain presence of interfacial oxide, as it affects:
        1) Growth mechanism.
        2) Contact resistivity.
    2) Account for J_{0c} differences between Ni and Al samples.

Presentation overview

Improved carrier selectivity of diffused silicon wafer solar cells

Majority carrier conductivity at p^+ and n^+ metal-silicon interfaces.

1. Exploiting the unintentional consequences of AlO_x wrap around on screen printed n^+ -silicon/Ag contact resistivity.
2. The properties of electroless nickel plated contacts to boron diffused p^+-silicon.

Characterising carrier selectivity at non-contacted diffused surfaces.

3. Understanding the surface recombination rate of diffused and inverted/depleted surfaces.
4. A novel method of extracting the surface recombination parameters from photoconductance measurements.

Applications to diffused homojunction IBC Solar cells

5. Fabrication and simulation solar cells results.

High injection behaviour at inverted surfaces

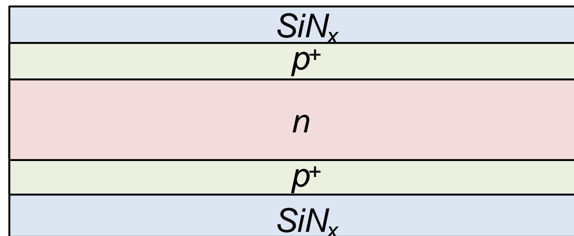

Relation proposed by Kane & Swanson[1]:

$$\frac{1}{\tau_{eff}} = \frac{1}{\tau_{bulk}} + 2\frac{J_0}{qn_i^2 W}\Delta n$$

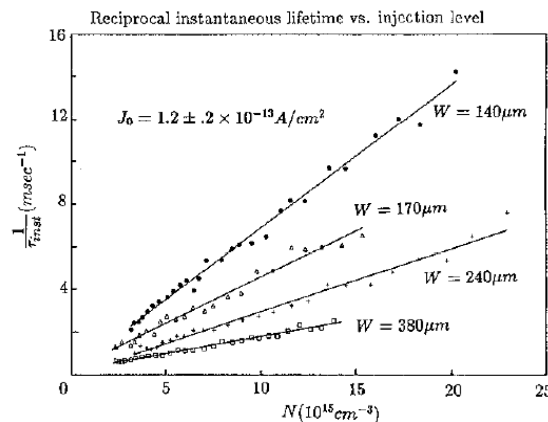

Fig. 7. - Test of the method. The extraction is carried out on wafers of different thickness having the same emitters.

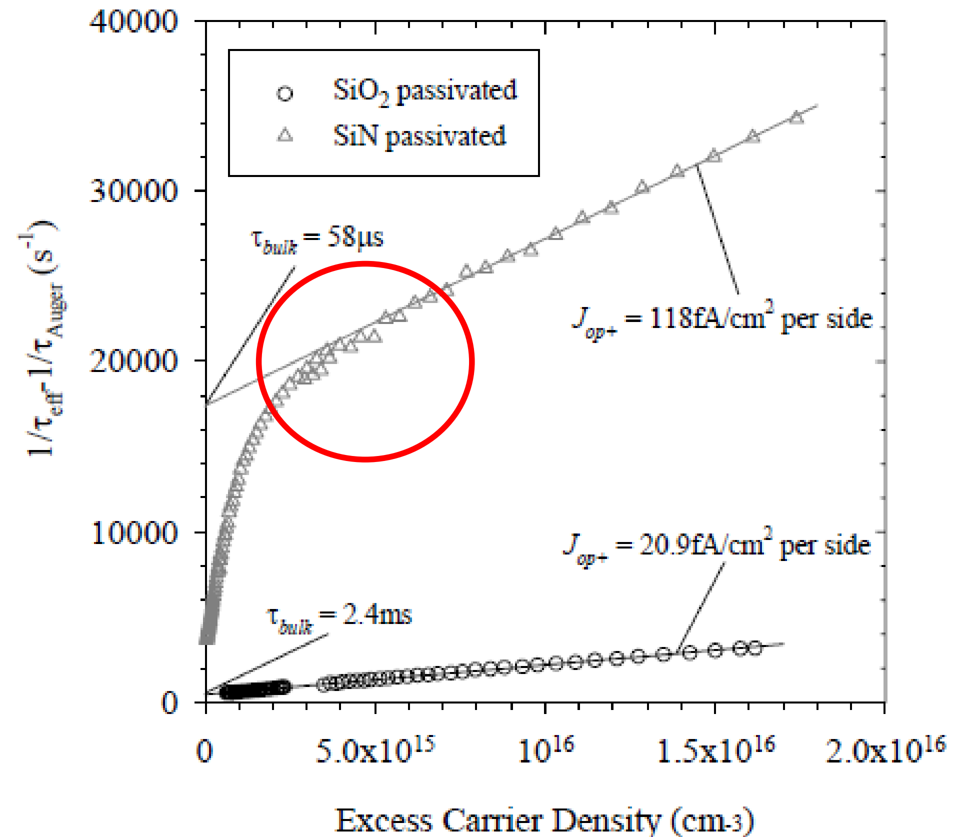

Figure 34 Injection level dependence of inverse lifetime for a p^+np^+ passivated sample with 150 Ω/□ diffusion.[2]

[1] D. E. Kane & R. M. Swanson, *IEEE PVSC*, (1985)

[2] M.J. Kerr, *Ph.D. Thesis*, (2002)

ARC Photovoltaics Centre of Excellence UNSW

UNSW
THE UNIVERSITY OF NEW SOUTH WALES
SYDNEY · CANBERRA · AUSTRALIA

Research

High injection behaviour at inverted surfaces

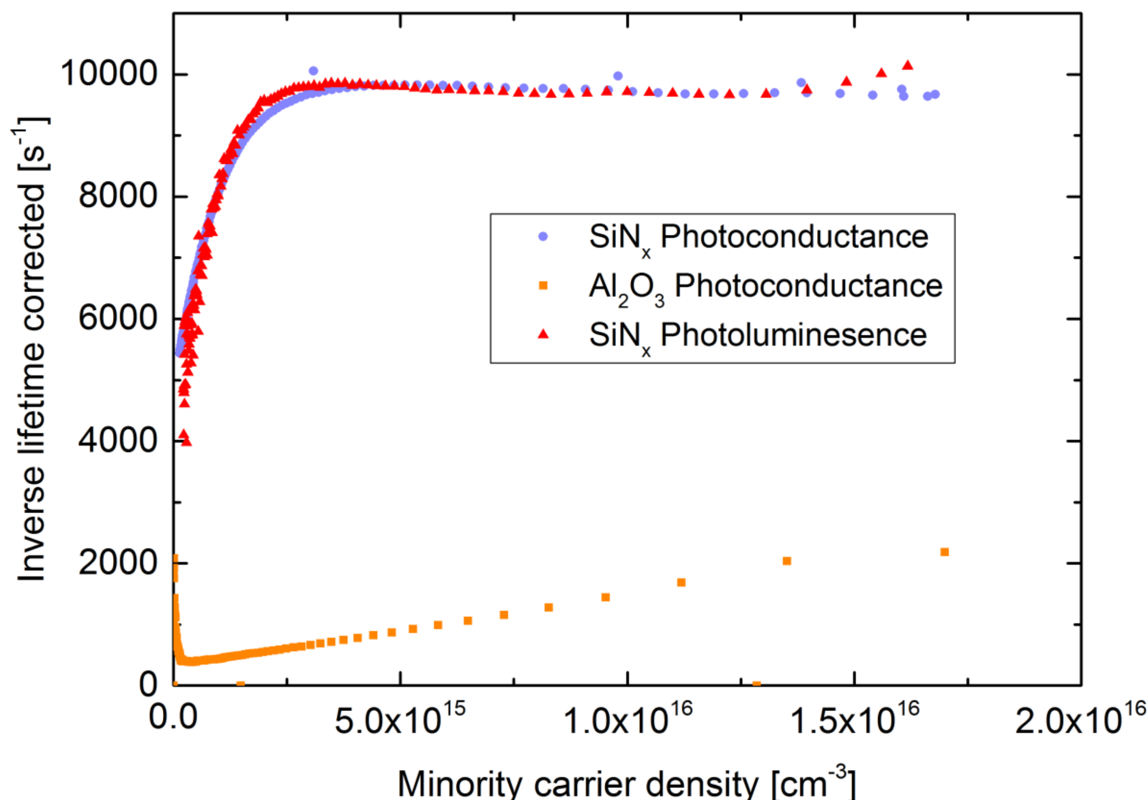

Figure 35 Measured inverse Auger corrected effective minority carrier lifetime of a lifetime sample featuring a symmetrical SiN_x-passivated p^+ surface. A measurement taken of a symmetrically diffused, Al_2O_3-passivated p^+ sample is shown for reference.

[1]To A. *et al.*, *J. J. App. Phys.*, ***56,*** *852* , 08MB05 (2016)

ARC Photovoltaics Centre of Excellence UNSW

UNSW THE UNIVERSITY OF NEW SOUTH WALES SYDNEY · CANBERRA · AUSTRALIA

High injection behaviour at inverted surfaces

Lifetime Simulation

Measured input data
- ECV active boron dopant profile
- Depth dependant generation rate
- Wafer thickness

Semiconductor Models
- Temperature
- Background doping
- Free carrier statistics
- Intrinsic carrier density
- Bandgap narrowing
- Mobility
- Auger recombination
- Radiative recombination
- Incident spectrum
- Optical properties of Silicon

Variables - Surface Recombination:
- Fixed charge Q_f
- Trap energy level E_{trap}
- Electron and hole capture cross section σ_n and σ_p
- Interface defect density D_{it}

SENTAURUS TCAD

Simulated Inverse lifetime curves

Key expressions[1]:

$$\tau_{eff} = \frac{\sigma_L}{J_{ph}(\mu_n + \mu_p)W}$$

$$\sigma_L = q\Delta n_{av}(\mu_n + \mu_p)W$$

$$U_{SRH} = \frac{p_s n_s - {n_{i,eff}}^2}{\dfrac{n_s + N_c e^{\frac{q}{KT}(E_{trap} - E_C)}}{D_{it}\sigma_n v_{th}} + \dfrac{p_s + N_v e^{\frac{q}{KT}(E_v - E_{trap})}}{D_{it}\sigma_p v_{th}}}$$

[1]Sinton, R. A., & Cuevas, A. *App. Phys. Lett.*, ***69***(17), (1996).

ARC Photovoltaics Centre of Excellence UNSW

UNSW THE UNIVERSITY OF NEW SOUTH WALES SYDNEY · CANBERRA · AUSTRALIA

High injection behaviour at inverted surfaces

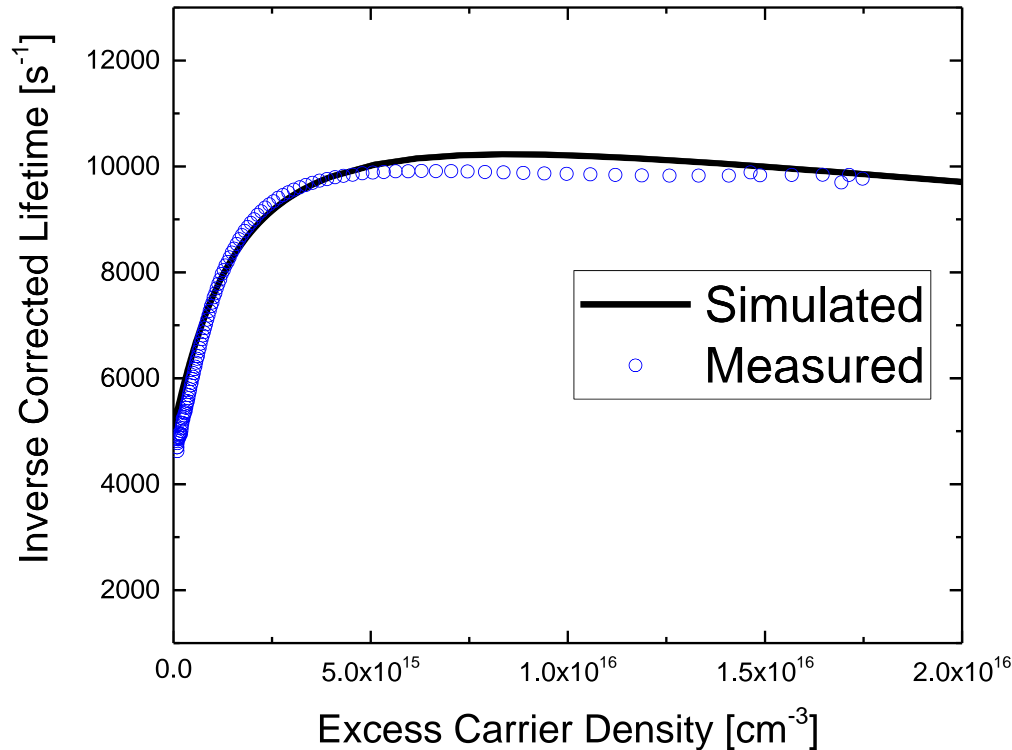

Figure 36 Simulated and measured injection inverse corrected lifetime curves of the symmetrical diffused structure used in this work. In this simulation D_{it}=7x10^{11} cm-3. Q_f = 3x10^{12} cm^{-3} and equal electron and hole capture rations of 10^{-17} cm/s.

[1]To A. *et al., J. J. App. Phys.*, ***56,*** *852* , 08MB05 (2016)

ARC Photovoltaics Centre of Excellence UNSW
UNSW THE UNIVERSITY OF NEW SOUTH WALES SYDNEY · CANBERRA · AUSTRALIA

Understanding the non-linearity

The result of a change in minority carrier concentration at the surface with increasing injection.

1. Case 1:
   Equilibrium and low injection where
   n_s, n_d << p_s , p_d

2. Case 2:
   'Moderate' injection
   where $n_s \approx p_s$

3. Case 3:
   High injection where
   $n_s > p_s$

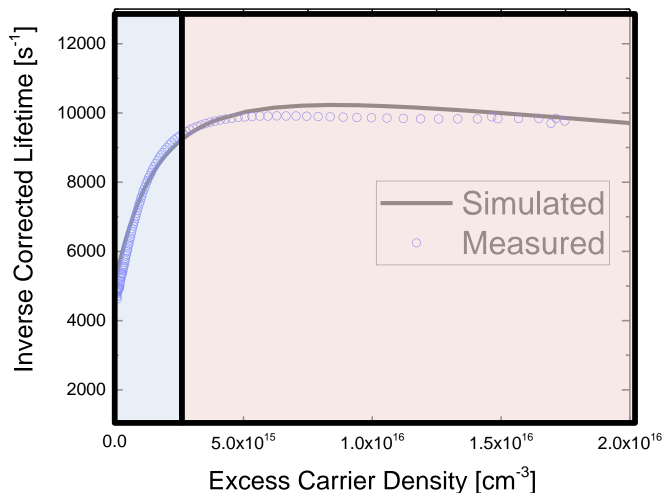

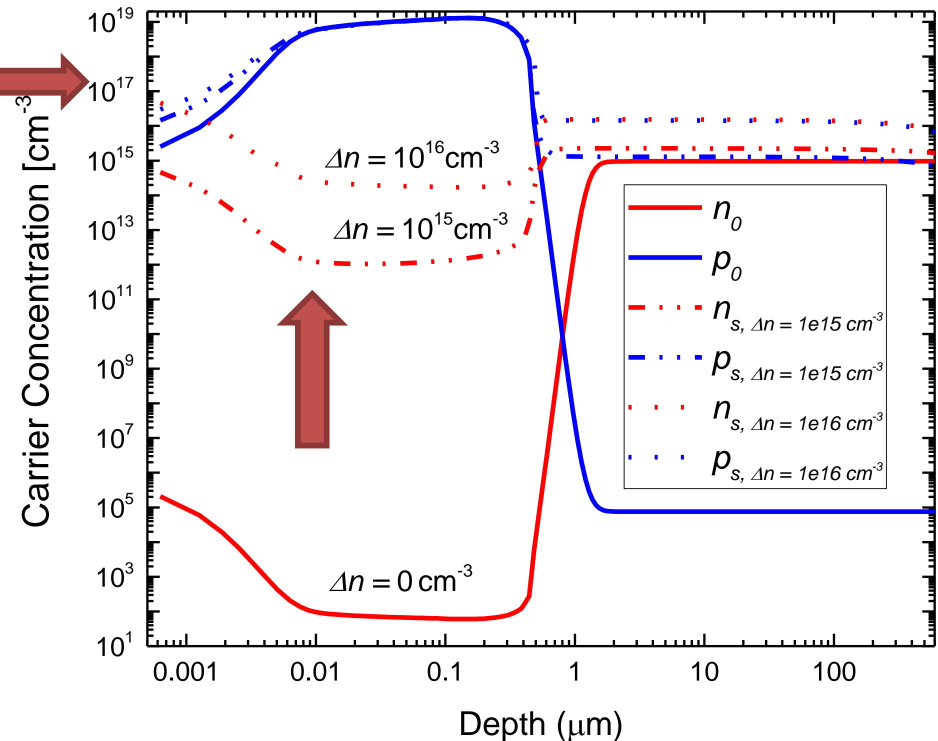

Figure 37 Cross sectional view of hole and electron concentration vs sample depth for increasing injection levels. In this simulation, D_{it}=7x10^{11} cm^{-3}, Q_f = 3x10^{12} cm^{-3} and $\sigma_n = \sigma_p$ = 10^{-17} cm/s

[1]To A. *et al., J. J. App. Phys.*, ***56,*** *852* , 08MB05 (2016)

ARC Photovoltaics Centre of Excellence UNSW
UNSW THE UNIVERSITY OF NEW SOUTH WALES SYDNEY · CANBERRA · AUSTRALIA

Quick Summary:

1) Non-linear behaviour a result of surface becoming inverted with increasing injection level.
2) This can be fitted using Sentaurus, and by using Q_f and D_{it} (or S_{n0}/S_{p0}) as free parameters.

Question: Can Q_f and or S_{n0}/S_{p0} be independently resolved?

→ Developed carrier statistics model to calculate n_s and p_s taking into account:

1) FD statistics.
2) Surface charge and band bending
3) Band-gap narrowing and degeneracy effects.

Key output: Relationship between Q, N_s and Δn and $U_{SRH, Surface}$.

Presentation overview

Improved carrier selectivity of diffused silicon wafer solar cells

Majority carrier conductivity at p^+ and n^+ metal-silicon interfaces.

1. Exploiting the unintentional consequences of AlO_x wrap around on screen printed n^+ -silicon/Ag contact resistivity.
2. The properties of electroless nickel plated contacts to boron diffused p^+-silicon.

Characterising carrier selectivity at non-contacted diffused surfaces.

3. Understanding the surface recombination rate of diffused and inverted/depleted surfaces.
4. A novel method of extracting the surface recombination parameters from photoconductance measurements.

Applications to diffused homojunction IBC Solar cells

5. Fabrication and simulation solar cells results.

ARC Photovoltaics Centre of Excellence UNSW
UNSW THE UNIVERSITY OF NEW SOUTH WALES SYDNEY · CANBERRA · AUSTRALIA

1. Surface band bending:

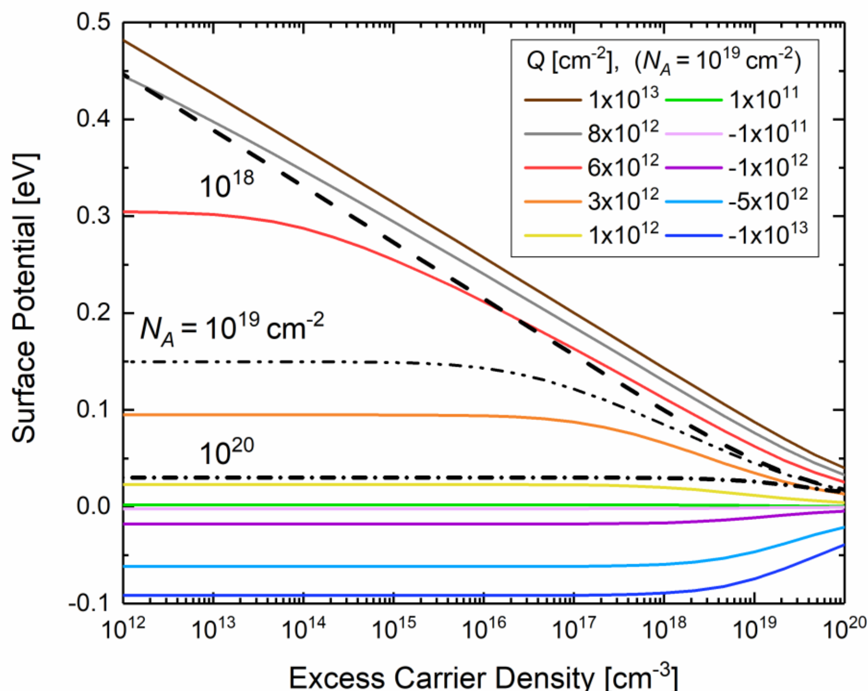

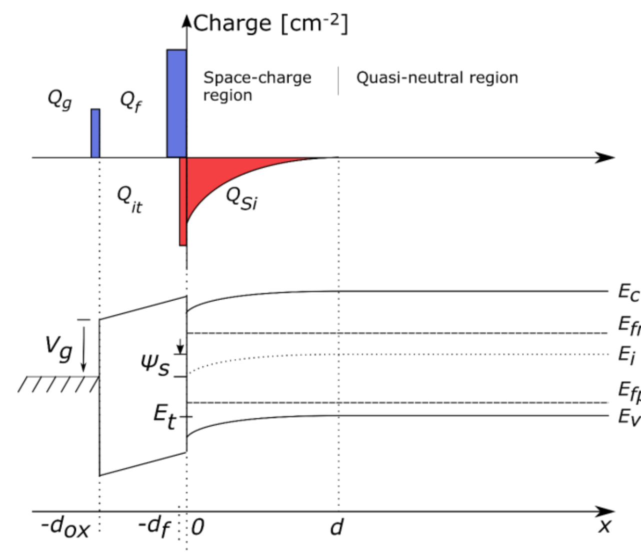

Figure 38 Surface potential as a function of excess carrier density, calculated using the method outlined in Ref. [39] for a range of net interface charge values (solid lines) with N_A=10^{19} cm^{-3}. Two curves with varying doping levels are simulated with $Q = 4\times10^{12}$ cm^{-2} (dashed lines) for comparison. In this plot, Schenck's BGN model and Fermi-Dirac statistics are used to calculate the carrier concentration at steady state.

ARC Photovoltaics Centre of Excellence UNSW
UNSW THE UNIVERSITY OF NEW SOUTH WALES SYDNEY · CANBERRA · AUSTRALIA

2. Surface carrier concentrations

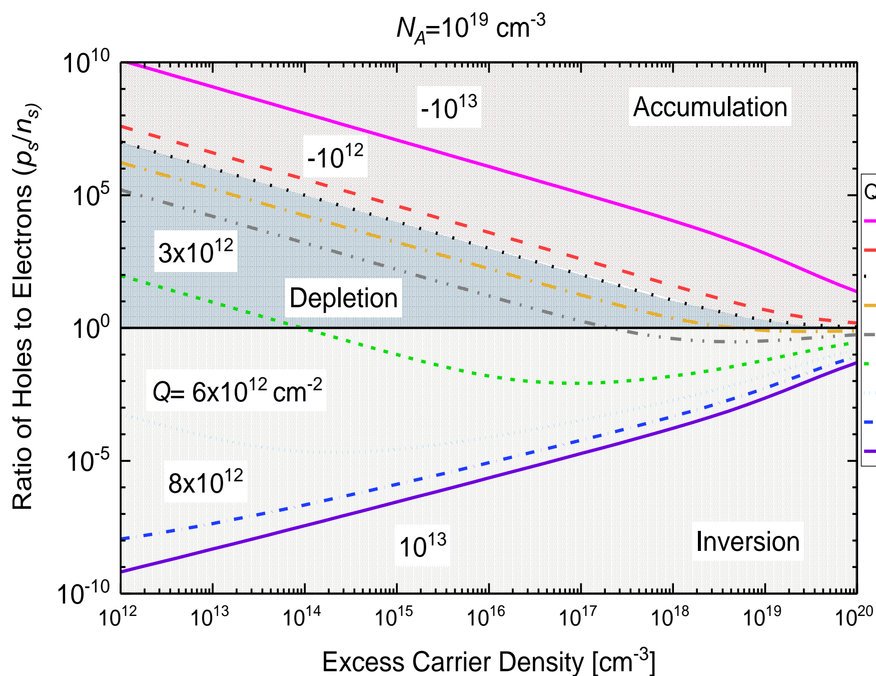

Figure 39 Ratio of holes to electrons, for a range of Q values, as a function of excess carrier density. The conditions where the surface condition is in accumulation, depletion or inversion are shaded, and the curves trace where surface condition transitions occur due to changing excess carrier density.

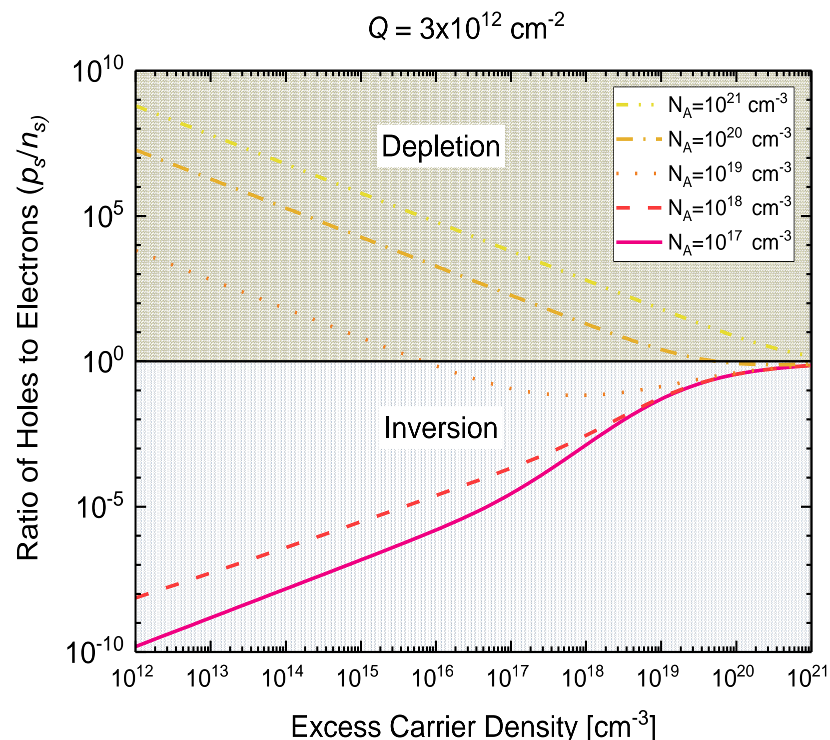

Figure 40 Ratio of holes to electrons, for a range of N_A values, as a function of excess carrier density. In these calculations, $Q = 3\text{x}10^{12}$ cm^{-3}. The conditions where the surface is in depletion or inversion are shaded, and the curves trace where transitions in surface condition occur due to changing excess carrier density.

3. Surface Recombination J_{0s}

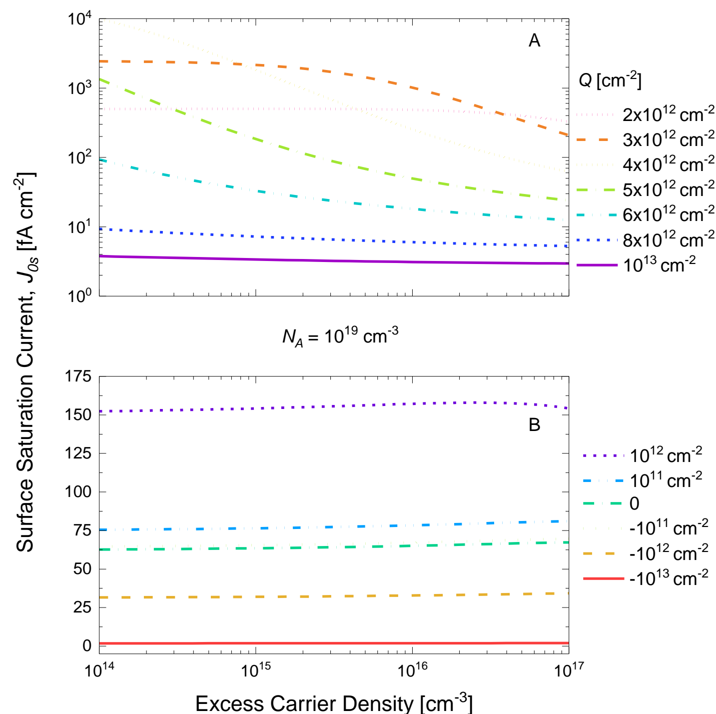

Figure 41 Calculated J_{0s} values as a function of excess carrier density, for a range of Q values. Plot A (top) shows that there is a range of values which produce a non-constant J_{0s} which produces non-linear inverse lifetime behaviour, whilst a range of positive and negative values produce the characteristic constant J_{0s} (bottom). These calculations are performed with $S_{n0} = S_{p0} =$ 5000 cm/s, a single trap level at the mid-gap for donors and acceptors, and acceptor doping density $N_A = 10^{19}$cm^{-3}.

ARC Photovoltaics Centre of Excellence UNSW
UNSW THE UNIVERSITY OF NEW SOUTH WALES SYDNEY · CANBERRA · AUSTRALIA

3. Surface Recombination J_{0s} – varying Q_f and S_{n0}/S_{p0}

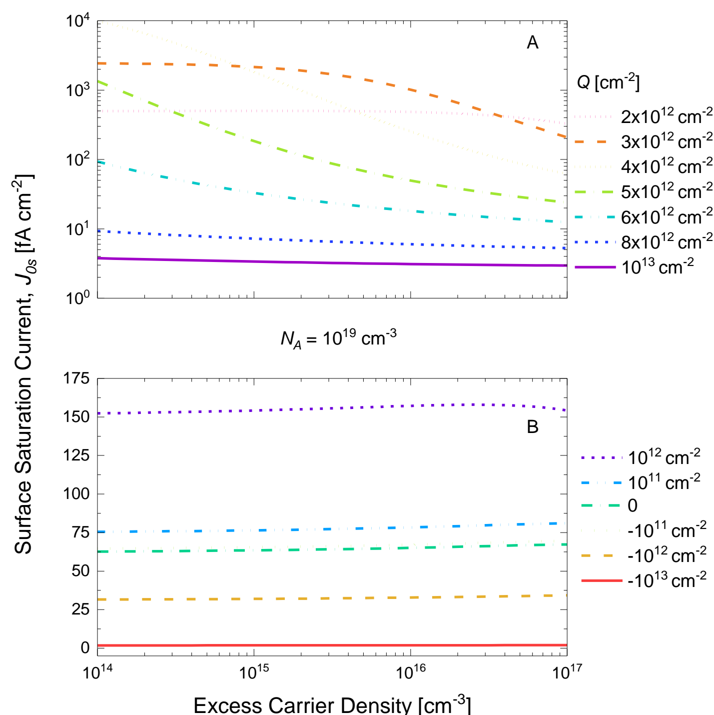

Figure 42 Calculated J_{0s} values as a function of excess carrier density, for a range of Q values. These calculations are performed with $S_{n0} = S_{p0} = 5000$ cm/s, a single trap level at the mid-gap for donors and acceptors, and acceptor doping density $N_A = 10^{19}$cm^{-3}.

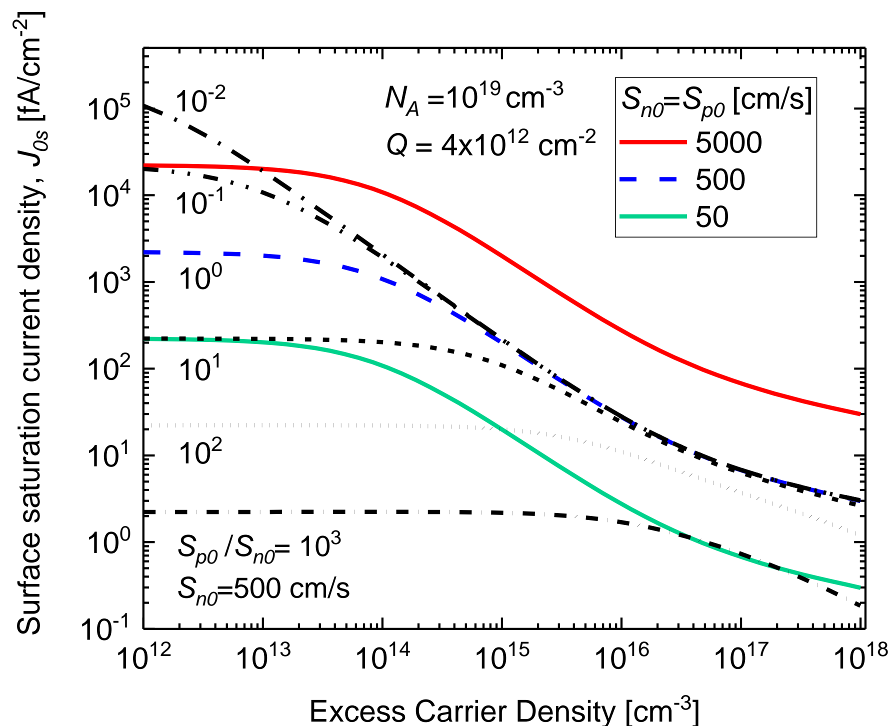

Figure 43 The effect of varying (coloured lines) and equal (dotted lines) S_{no} and S_{po} values on J_{0s}, for a p-doped surface with $N_A = 10^{19}$ cm^{-3} and $Q = 4\times10^{12}$ cm^{-2}.

ARC PHOTOVOLTAICS CENTRE OF EXCELLENCE UNSW
UNSW THE UNIVERSITY OF NEW SOUTH WALES SYDNEY · CANBERRA · AUSTRALIA

Results – Thermal Annealing

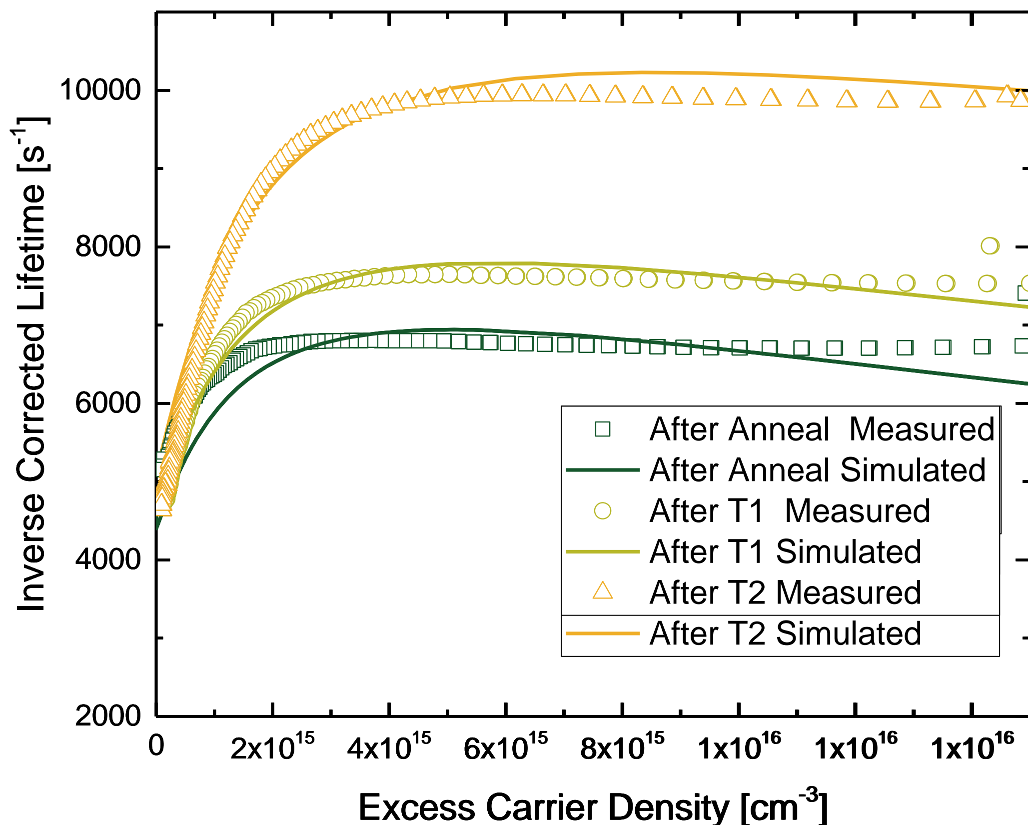

Figure 44 Measured vs. fitted inverse lifetime curves after various thermal anneal treatments. The fitted data is simulated in SENTAURUS with equal electron and hole capture cross sections of 10^{-17} cm/s.

Extracted Interface Values

Process	D_{it} [cm^{-2}]	Q_f [cm^{-2}]
Annealed	4.8×10^{11}	3.2×10^{12}
Anneal Treatment 1 (T1)	5.5×10^{11}	3.2×10^{12}
Anneal Treatment 2 (T2)	7.5×10^{11}	3.2×10^{12}

ARC Photovoltaics Centre of Excellence UNSW
UNSW The University of New South Wales Sydney · Canberra · Australia

Results – Negative Charging

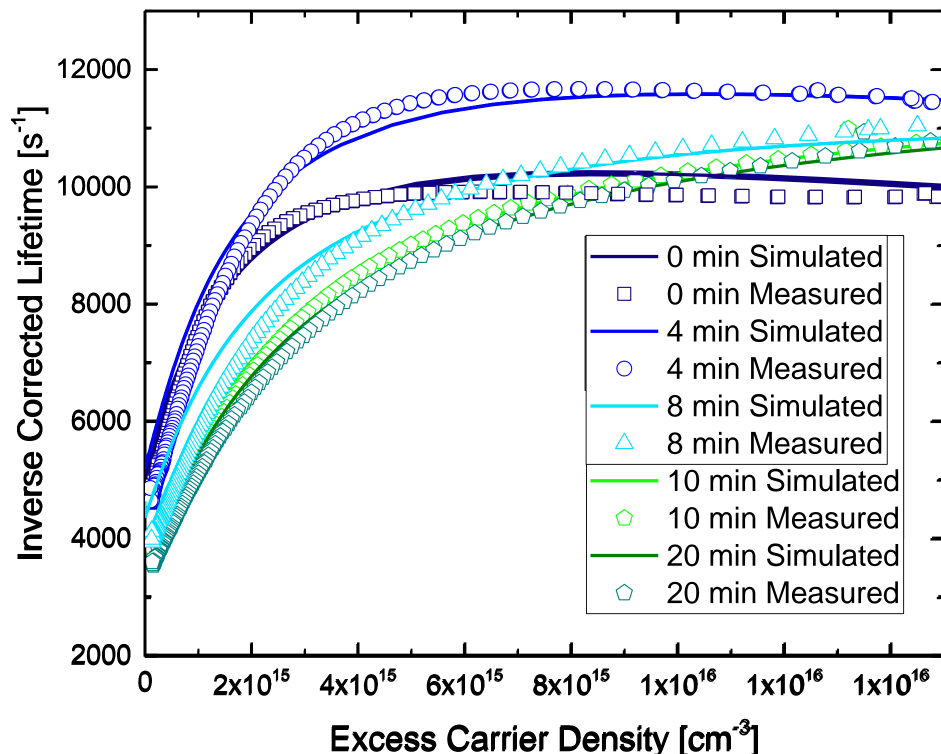

Figure 45 Measured vs. fitted inverse lifetime curves after various durations of corona charge. The time intervals represent the amount of charging per side. The fitted data is simulated in SENTAURUS with equal electron and hole capture cross sections of 10^{17} cm/s.

Extracted Interface Values

Charging Time [min]	D_{it} [cm^{-2}]	Q_f [cm^{-2}]
0 min	7.5×10^{11}	3×10^{12}
4 min	8.6×10^{11}	3×10^{12}
8 min	7.5×10^{11}	2.6×10^{12}
10 min	7.5×10^{11}	2.4×10^{12}
20 min	7.5×10^{11}	2.35×10^{12}

ARC Photovoltaics Centre of Excellence UNSW
UNSW THE UNIVERSITY OF NEW SOUTH WALES SYDNEY · CANBERRA · AUSTRALIA

1. General conditions:

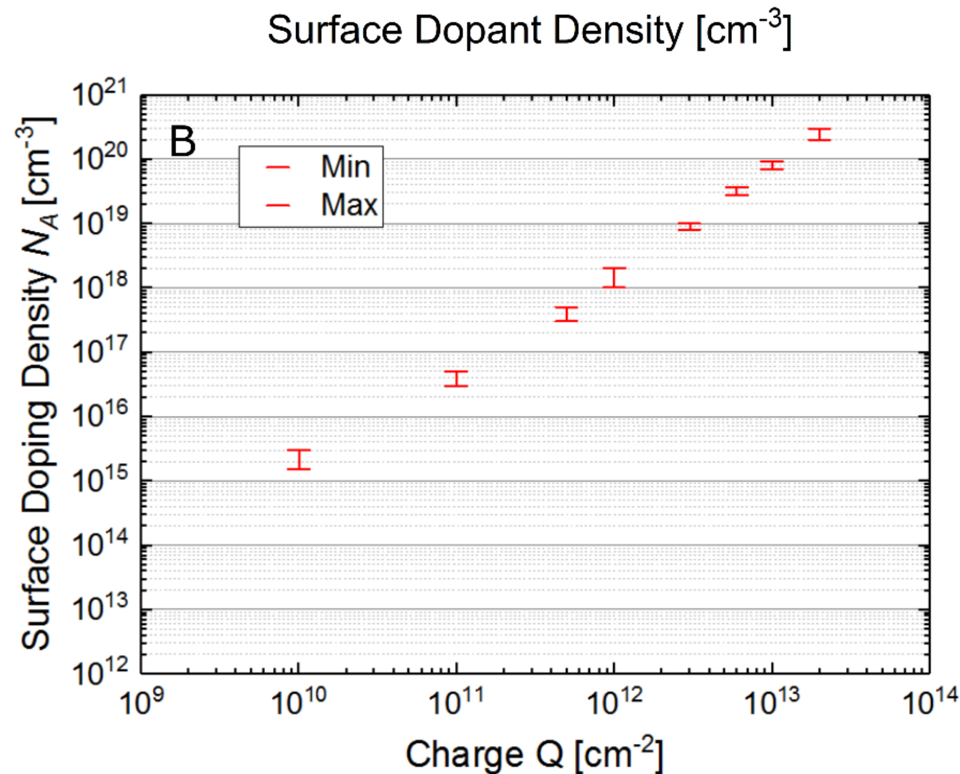

Figure 46 The surface doping and charge ranges whereby a surface transition from depletion to inversion condition will occur between $\Delta n = 10^{15}\text{cm}^{-3}$ and $\Delta n = 10^{16}\ \text{cm}^{-3}$.

Fitting examples

HfO_x/p-type

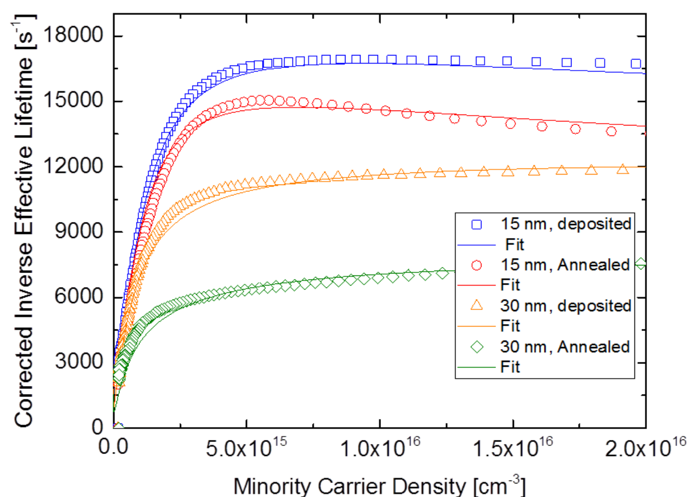

Table 4 Extracted interface parameters from HfO_x passivated samples.

Thickness	Parameter	Deposited	After Anneal
15 nm	Q	1.4x10^{12} cm^{-2}	1.8x10^{12} cm^{-2}
	S_{n0}	135 cm/s	152 cm/s
30 nm	Q	3x10^{11} cm^{-2}	2x10^{11} cm^{-2}
	S_{n0}	65 cm/s	40 cm/s

AlO_x/n-type

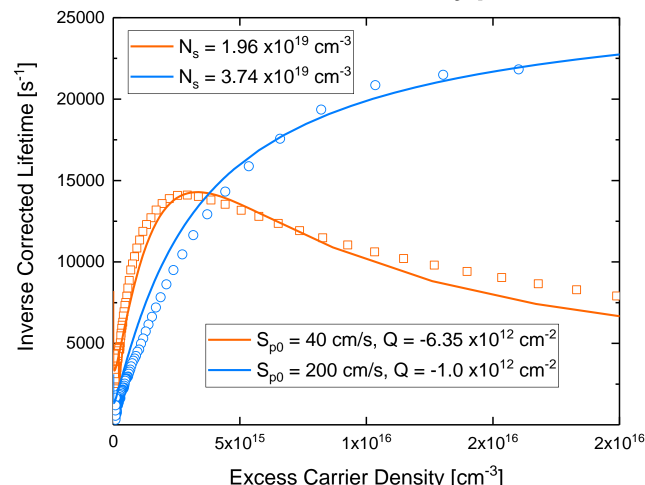

Table 5 Extracted interface parameters from AlO_x passivated samples.

Sample	S_{n0} [cm/s]	Q [cm^{-2}]
A	40	-6.35 ×10^{12}
B	200	-1.0×10^{12}

ARC Photovoltaics Centre of Excellence UNSW
UNSW THE UNIVERSITY OF NEW SOUTH WALES SYDNEY · CANBERRA · AUSTRALIA

Presentation overview

Improved carrier selectivity of diffused silicon wafer solar cells

Majority carrier conductivity at p^+ and n^+ metal-silicon interfaces.

1. Exploiting the unintentional consequences of AlO_x wrap around on screen printed n^+ -silicon/Ag contact resistivity.
2. The properties of electroless nickel plated contacts to boron diffused p^+-silicon.

Characterising carrier selectivity at non-contacted diffused surfaces.

3. Understanding the surface recombination rate of diffused and inverted/depleted surfaces.
4. A novel method of extracting the surface recombination parameters from photoconductance measurements.

Applications to diffused homojunction IBC Solar cells

5. Fabrication and simulation solar cells results.

ARC Photovoltaics Centre of Excellence UNSW

UNSW THE UNIVERSITY OF NEW SOUTH WALES SYDNEY · CANBERRA · AUSTRALIA

Diffused Homojunction IBC solar cells

Development of an IBC for advanced light-trapping structures

Collaboration between UNSW and University of Southampton

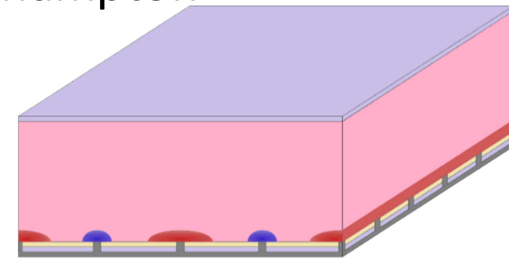

- Historically among the highest efficiencies, but also the most expensive
  - Current world-record Si cell is a heterojunction IBC cell at ~26.7% (Kaneka)
- Thinner cells may possess higher V_{0c}'s, provided there is excellent passivation and light trapping
- Most significant loss factor in SunPower cells is poor light trapping
- IBC design is especially attractive for research on thin cells and front surface light trapping
  - Largely decouples the optimisation of optical and electrical properties
  - Can easily modify fully processed cells

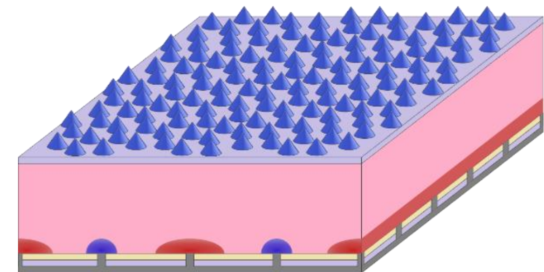

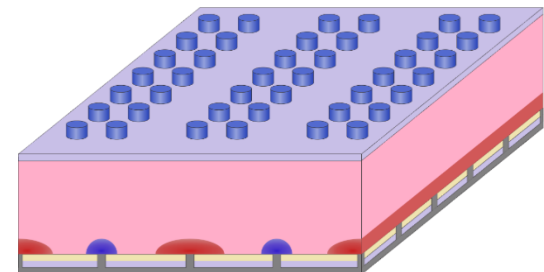

Diffused Homojunction IBC solar cells

- Processing sequence:

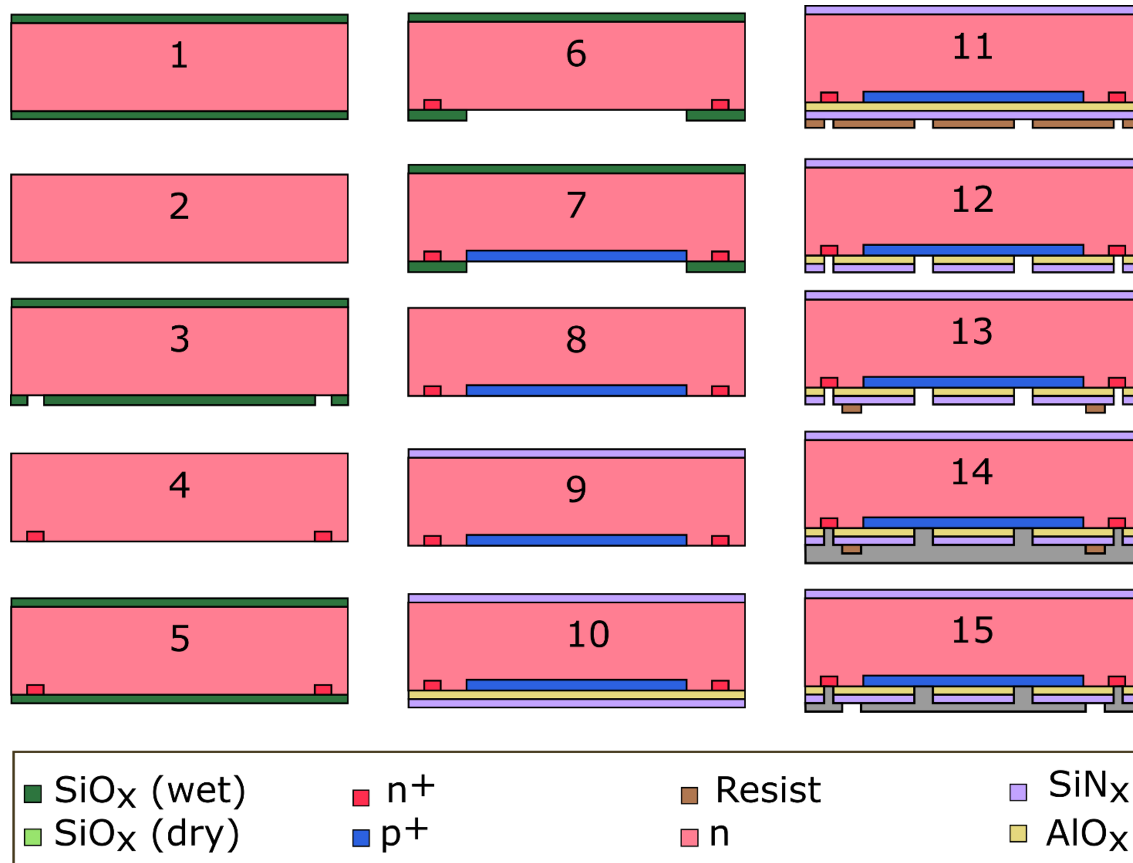

Processing issues: E-Beam evaporation RIE damage, Bulk Stabilisation

PL Image Analysis

a) PL image of a wafer after e-beam evaporation, pre (left) and post (right) sintering.
b) PL image of a wafer repassivated after one half was subject to RIE exposure (right) whilst the other side was masked from RIE exposure (left).
c) PL image of wafer using buffered HF etch (left) and RIE etch (right) passivated with AlO_x after boron diffusion.
d) PL image of wafer without (left, Cell A) and with (right, Cell B) bulk FZ treatment. All wafers are 4" in diameter. All images are at 1 sun, with exposure times of 1s for (a) and 0.1s for (b), (c), and (d), and have been deconvolved using PL Pro

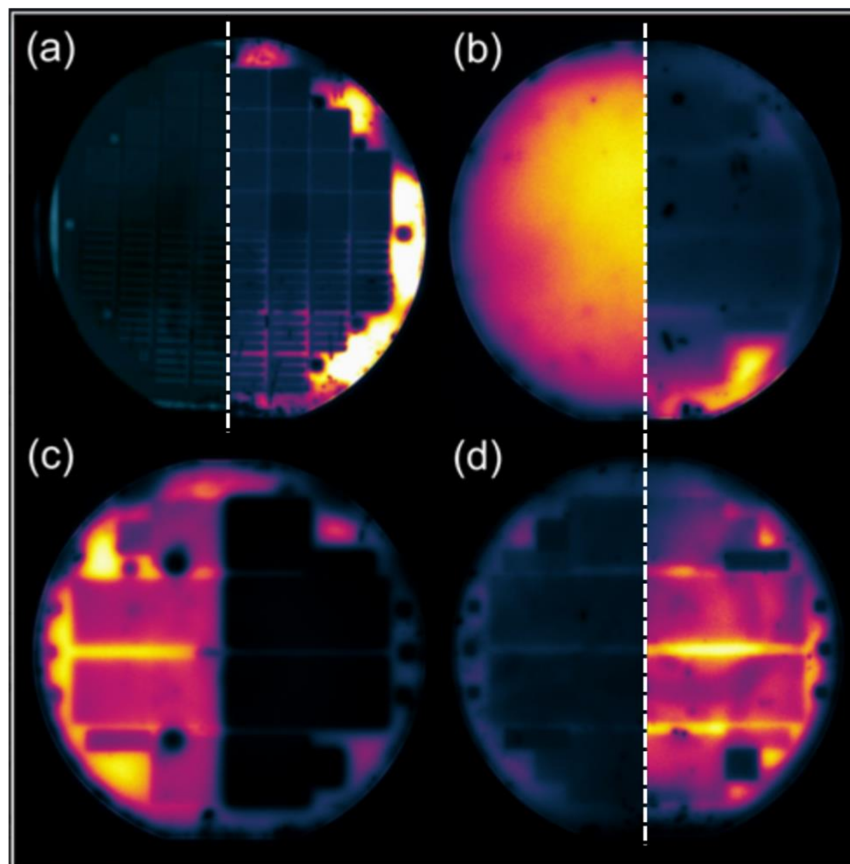

Figure 48 PL images of partially processed wafers, showing the effect of various processes.

Rahman, T., To, A., M. Pollard et al. *PIPV*, (2017))

Processing issues: 1. RIE Damage, Bulk Stabilisation

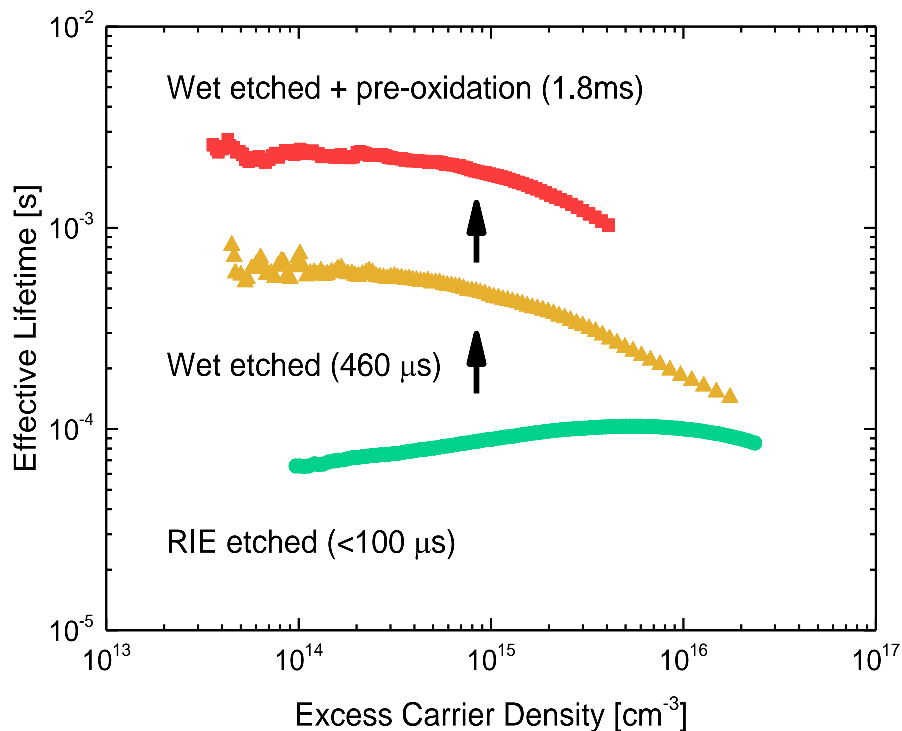

Figure 49 Measured effective minority carrier lifetime of cells on FZ 3.2 Ω-cm *n*-type silicon wafer (prior to metallisation) for RIE etched cells, wet etched cells (Cell A) and wet etched cells with bulk FZ treatment (Cell B).

Diffused Homojunction IBC solar cells

Parameter	Cell B 18.3 %	Characterisation method description
Cell thickness	280 µm	Measured with micrometer
Wafer resistivity	2.5 Ω.cm	Measured via PC dark conductance
Bulk SRH Lifetime	5 ms	PC measurement (see Appendix A)
p^+ surface concentration $N_{A,s}$	1.4×10^{-19} cm^{-3}	Four-point probe calibrated ECV
p^+ R_{Sheet}	114 Ω/□	Four-point probe measurement
p^+ J_{0e}	18.95 fA/cm^2	PC measurement on process monitor
p^+contact J_{0c}	1160 fA/cm^2	Simulated in EDNA2 [82], with the ECV profile input and $S = 10^7$ cm/s
p^+ contact resistivity ρ_c	3.6 mΩ.cm^2	CTLM measurement
n^+ surface concentration $N_{D,s}$	4.3×10^{-19} cm^{-3}	Four-point probe calibrated ECV
n^+ R_{sheet}	26 Ω/□	Four-point probe measurement
n^+ J_{0e}	160 fA/cm^2	PC measurement on process monitor
n^+ contact J_{0c}	186 fA/cm^2	Simulated in EDNA2 [82], with the ECV profile input and $S=10^7$ cm/s
n^+ contact resistivity ρ_c	0.76 m Ω.cm^2	CTLM measurement
Rear undiffused J_{0s}	2.89 fA/cm^2	PC measurement on process monitor
Front undiffused J_{0s}	8.55 fA/cm^2	PC measurement on process monitors
Reflection	Planar	UV-VIS measurement, generation profile extracted using OPAL2[97]

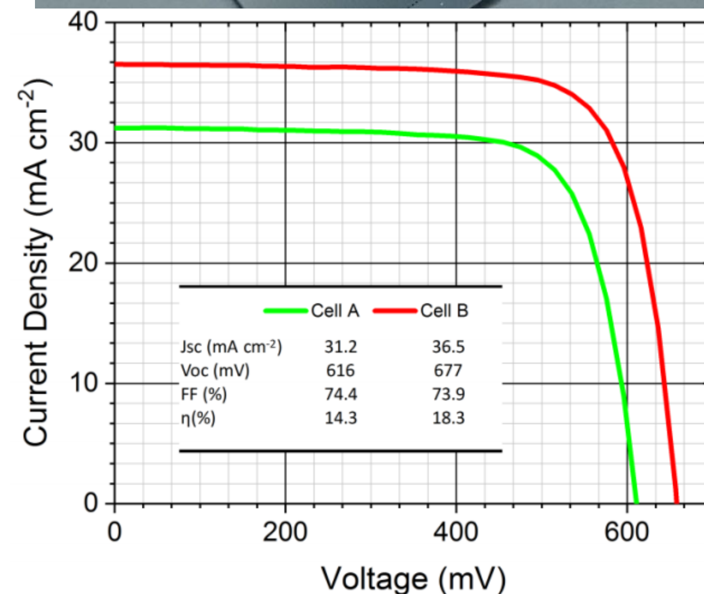

Rear surface passivation of diffused surfaces

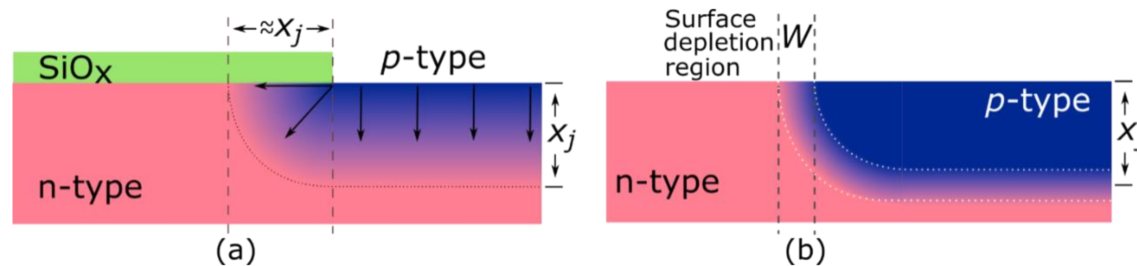

Figure 50 Schematic depiction of the formation of a surface depletion. The left image (a) depicts the formation of the localised metallurgical junction of depth x_j during an SiO_x masked thermal diffusion. This leads to the formation of a depletion region of width W within the device at and at the surface (b).

Research

Diffused Homojunction IBC solar cells

Rear J_{0s}

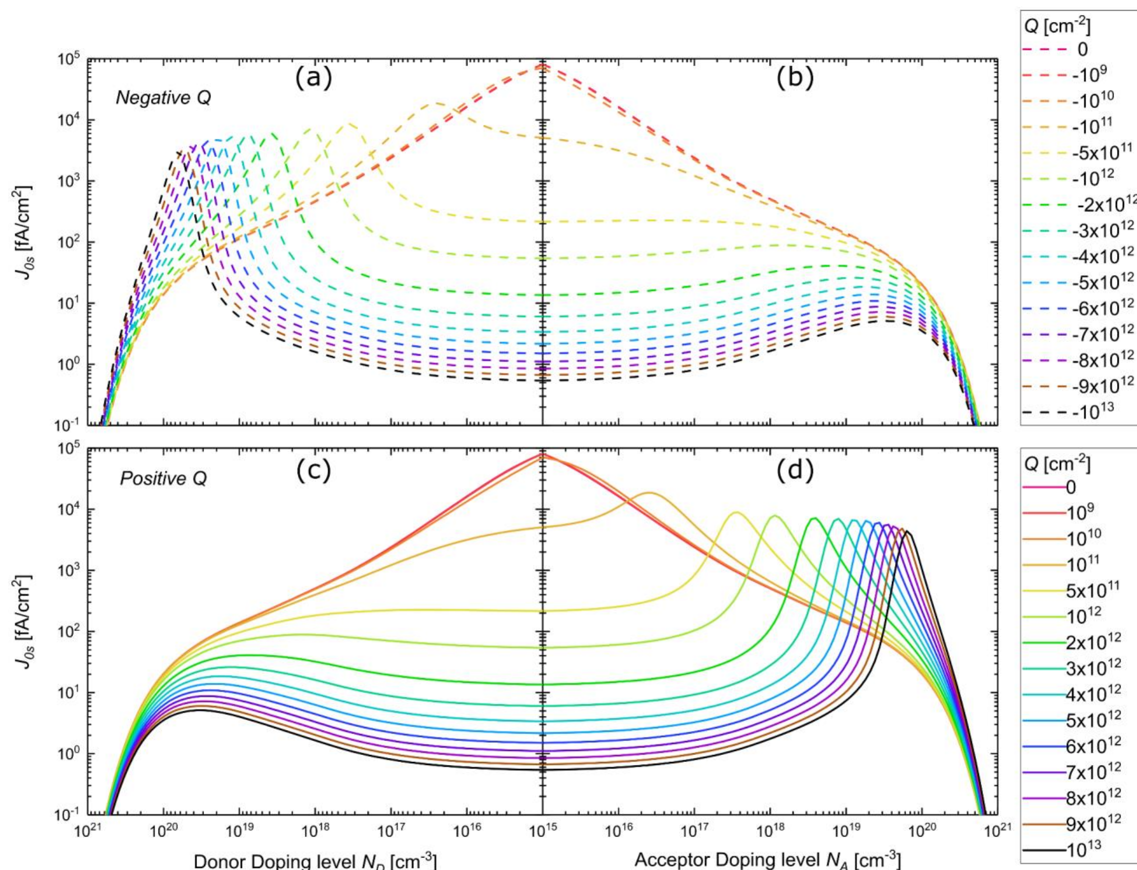

Figure 51 Rear surface J_{0s} as a function of doping level and Q calculated Δn = 10^{15} cm^{-3}, taking into account Fermi-Dirac statistics, band gap narrowing and degeneracy. The values of J_{0s} were calculated with S_{n0}=S_{p0}=10^4 cm/s for a single mid-band gap trap state. Electrostatics at the interface were solved analytically according to the Girish model

ARC Photovoltaics Centre of Excellence UNSW

UNSW
THE UNIVERSITY OF NEW SOUTH WALES
SYDNEY · CANBERRA · AUSTRALIA

Rear surface U_{srh}:

Sentaurus Simulations:

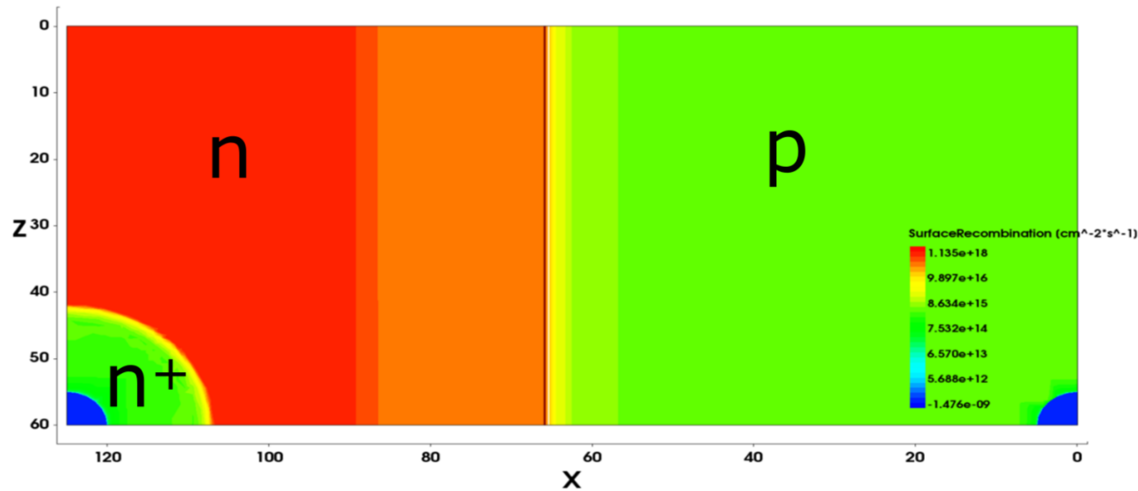

Figure 52 Spatial map of the surface recombination rate on the rear side of the simulated IBC solar cell, calculated and visualised in Sentaurus with rear $Q = -10^{11}$ cm^{2}

ARC Photovoltaics Centre of Excellence UNSW
UNSW THE UNIVERSITY OF NEW SOUTH WALES SYDNEY · CANBERRA · AUSTRALIA

Rear Surface Passivation

Sentaurus Simulations:

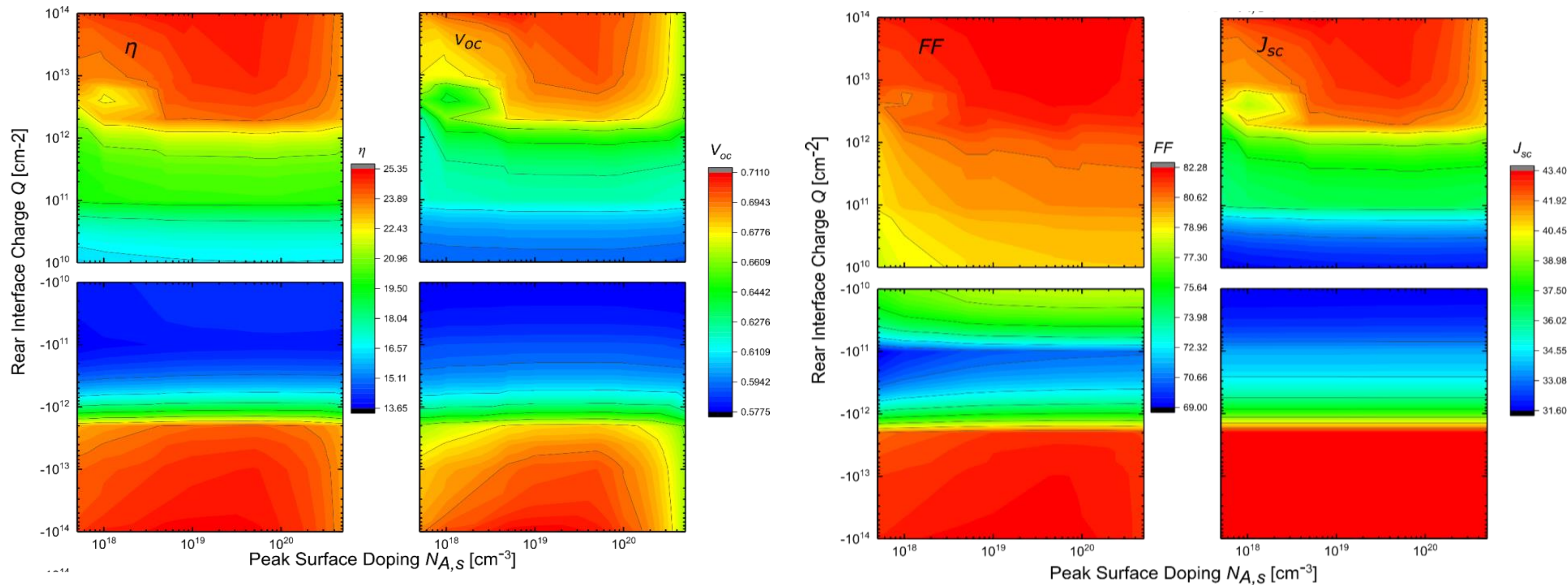

Figure 53 Simulated efficiency (a), V_{oc} (b), *FF* (c) and J_{sc} (d) of a diffused homojunction IBC solar cell for a range of rear Q values, S = 5000 cm/s.

Rear Surface Passivation:

Effect of varying rear *S*

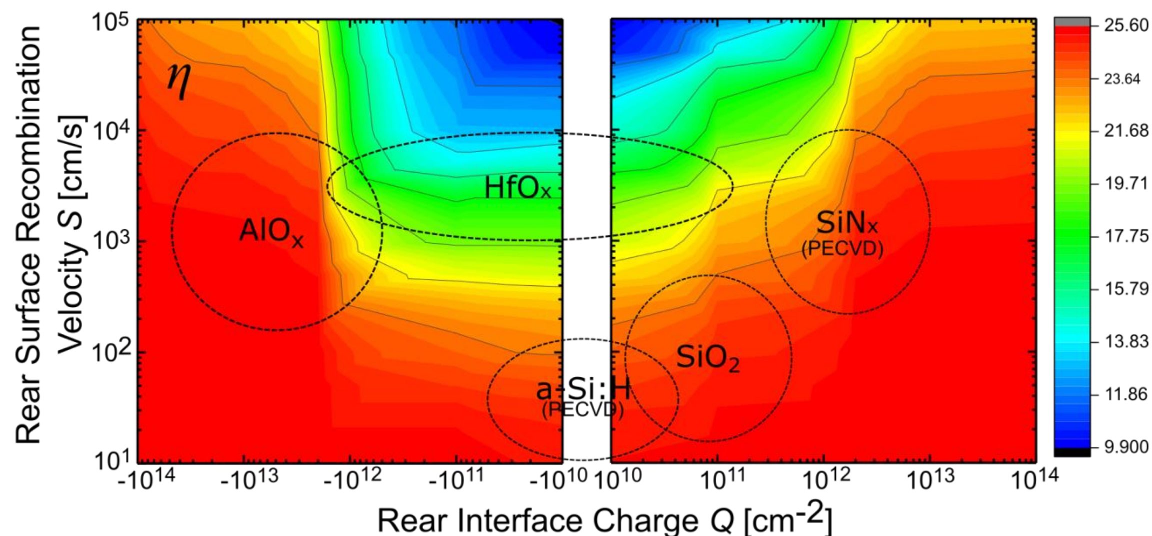

Figure 54 Conversion efficiency of a diffused homojunction IBC solar cell for a range of rear *S* and *Q* values, with typical interface values of a range of dielectrics, sourced from [340] imposed over the image to indicate the potential performance of an actual cell fabricated with those materials on the rear.

Quokka simulated nickel plated solar cells

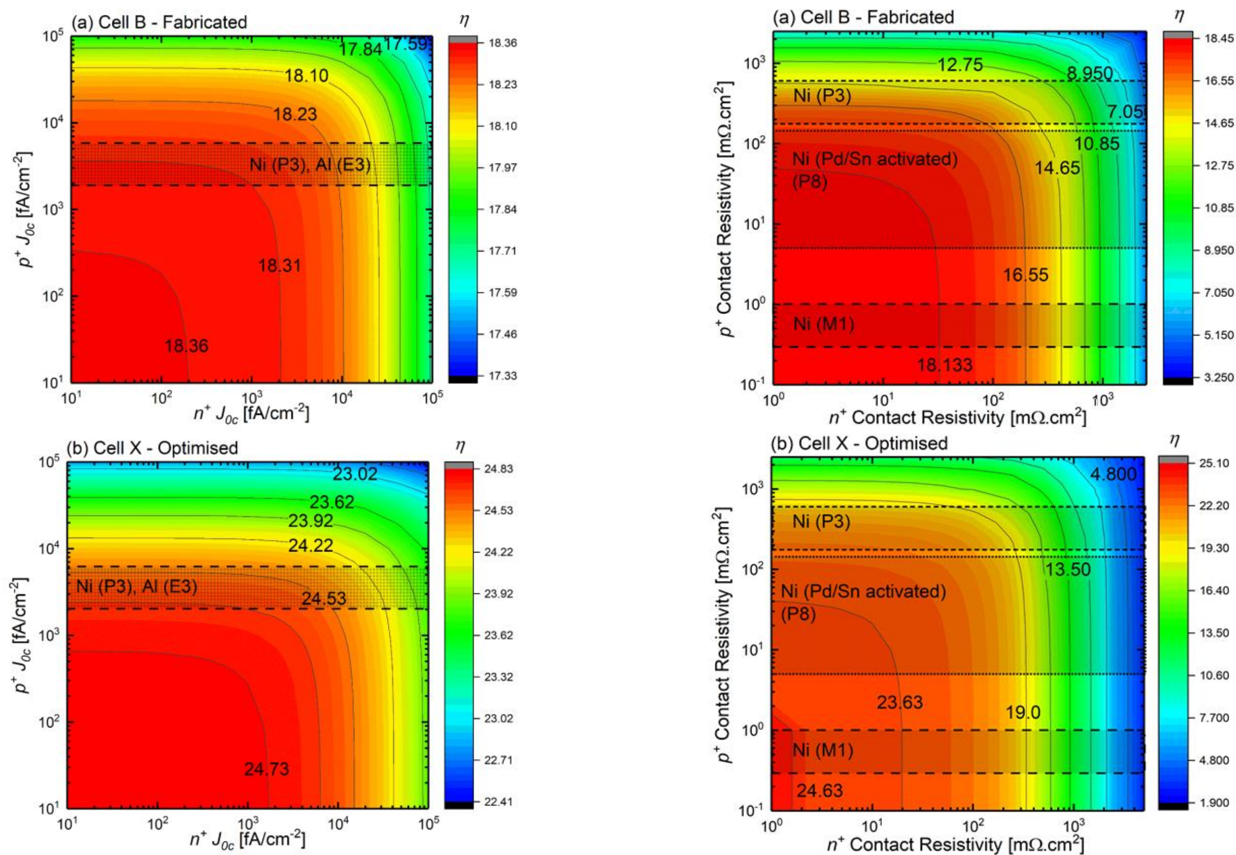

Figure 55 Simulated efficiency curves for various rear contact metallisation schemes.

ARC Photovoltaics Centre of Excellence UNSW

UNSW THE UNIVERSITY OF NEW SOUTH WALES SYDNEY · CANBERRA · AUSTRALIA

Summary

IBC Solar Cells

1. Careful processing required to avoid bulk and surface damage during IBC solar cell processing.
2. AlO_x and SiN_x may effectively be used to passivated the rear of high performance IBC solar cells.

Surface recombination modelling

1. A novel method of extracting the interface parameters from diffused surfaces using PC measurements has been demonstrated.

Electroless Nickel Contacts

1. Significant potential for low resistivity contacts.
2. More work is required to improve process repeatability, and understand the differences between Al and Ni contact J_{0c} and ρ_c

Electroless Nickel Contacts

1. Significant potential for low resistivity contacts.
2. More work is required to improve process repeatability, and understand the differences between Al and Ni contact J_{0c} and ρ_c

Future Work

IBC Solar Cells

1. Cell fabrication
    1. Different rear surface dielectrics.
    2. Gettering of impurities to avoid further bulk lifetime degradation.

Surface recombination modelling

1. Expand model to take into account further effects
2. Develop a freeware software model to enable external researchers to perform fitting and extraction.

Electroless Nickel Contacts

1. TEM imaging of interface.
2. Experiment repeats to troubleshoot repeatability issues.

AlO_x wrap around.

1. Investigate cause of improved contact resistivity.

Acknowledgements:

Supervisors: Bram Hoex and Alison Lennon.

Collaborators: F.J. Ma, M. Pollard, T. Rahman, R. Davidsen, A. Garavaglia, S. Tahir, J. Rodriguez, J. Colwell, N. Nampalli, H.Z. Li, X.R. An, A. Han, C. Johnson, D. Payne + Bram's Group.

ANFF Team (Linda Macks, Ute Schubert)
SIRF Team (Kyung, Ly Mai, Nino)
LDOT (Kian, Nick, Alan, Mark, Tom)

ARENA (Scholarship funding)

All the wonderful people at SPREE!!

UNSW
THE UNIVERSITY OF NEW SOUTH WALES
SYDNEY · CANBERRA · AUSTRALIA

Thank you

e-mail: alexander.to@unsw.edu.au